A MICROMECHANICS APPROACH TO THE STUDY OF HYDROGEN TRANSPORT AND EMBRITTLEMENT

A. Taha and P. Sofronis
Department of Theoretical and Applied Mechanics
University of Illinois at Urbana-Champaign
104 South Wright Street
Urbana, Illinois, 61801

January 1999

Abstract

The mechanisms of hydrogen related fracture are briefly outlined. Previous investigations on the physics and treatment of the hydrogen transport processes are reviewed. A hydrogen diffusion model based on the interaction of hydrogen induced strain in the lattice with local material elastoplasticity is presented. Finite element studied were carried out to analyze the hydrogen distribution in the neighborhood of a blunting crack tip under small scale yielding conditions and in the neighborhood of a rounded notch in a 4-point bend specimen. The calculated hydrogen concentration profiles and experimental observations of embrittlement in high strength steels are used to make evaluative statements on the occurrence of the first microcracking event.

1. INTRODUCTION

Hydrogen embrittlement is a severe environmental type of failure [1-9]. When hydrogen is present, materials fail at load levels that are very low compared with those that a hydrogen free material can sustain. The result is usually catastrophic fracture which occurs unexpectedly, sometimes after many years of service [10]. Embrittlement can occur due to hydrogen contained in a pressure vessel or arising from chemical reactions.

Despite extensive study, the mechanism(s) of hydrogen embrittlement has remained unclear. Several candidate mechanisms have evolved, each of which is supported by sets of experimental observations and strong personal views. One reasonable certain aspect of this controversy is that there are several viable mechanisms of hydrogen related failure and that the search for a single mechanism to explain all observations is doomed to failure [1, 8, 11]. Of the many suggestions,

three mechanisms appear to be viable; stress induced hydride formation and cleavage [12-18], hydrogen enhanced localized plasticity [1, 8, 19-25], and hydrogen induced decohesion [26-32]. The first of these has been definitively established to be operative in systems in which hydrides are either stable, or can be stabilized by the application of a stress field, e.g. Group Vb metals [14, 33-35], Ti [16, 36], and, Zr [37]. This "second phase" mechanism is supported by microscopic observations [38] and thermodynamic calculations [13, 39]. In these hydride forming systems it has been shown [16] that under conditions in which the hydride cannot form, hydrogen "embrittlement" will occur by the second mechanism named above, hydrogen enhanced localized plasticity. The hydrogen enhanced localized plasticity mechanism is based on observations that in a range of temperatures and strain rates, the presence of hydrogen in solid solution decreases the barriers to dislocation motion, thereby increasing the amount of deformation that occurs in a localized region adjacent to the fracture surface [40-46]. The fracture process is a highly localized plastic failure process rather than an embrittlement. This counterintuitive process says that the macroscopic ductility is limited by the onset of extensive localized plasticity and is supported by microscopic observations. The third viable mechanism is the hydrogen related decohesion mechanism in which the atomic bonding at the crack tip is weakened by the presence of hydrogen in solid solution [26-32]. This mechanism is supported primarily by the observations that in some non-hydride forming systems, hydrogen embrittlement appears to occur in the absence of significant local deformation, by theoretical calculations of the effect of hydrogen on the atomic potentials [47] and by a thermodynamic argument [48-49].

A very important aspect of hydrogen embrittlement is that there exists a transport stage [7] of hydrogen to the sites where degradation occur. The ductility minimum versus temperature [5] (at low temperatures hydrogen diffusion slows whereas at high temperatures, stress levels and thermodynamics do not allow for

critical hydrogen concentrations to be achieved), the increase in ductility with increased strain rate (hydrogen cannot diffuse effectively), the incubation period, and the critical hydrogen concentration build-up before fracture are all important features that reflect transport kinetics [1] rather than mechanisms of failure. Therefore, the analysis of the hydrogen transport processes should precede any attempt to address the issue of hydrogen embrittlement related failures [2].

The purpose of this work is to review the progress to date in analyzing the material mechanical behavior at a crack tip [50-52] or a rounded notch [53] with that of hydrogen diffusion. An effort is made to address the role of significant parameters according to experimental findings, e.g. hydrostatic stress, plastic strain, and hydrogen concentration. Hydrogen concentrations predicted in conjunction with a continuum plasticity viewpoint are then used to correlate experimental observations on crack initiation. In the interest of clarity and economy, the systems that are investigated either do not form hydrides (steels, Fe and Ni) or, if they form hydrides as is the case of niobium, the initial concentration of hydrogen is chosen small enough so that no hydride precipitation is favored under the given loading and temperature conditions. A detailed presentation of the micromechanical treatment of hydrogen transport and diffusion in the presence of hydride formation can be found in the recent work of Lufrano *et al.* [17, 18].

2. PHYSICS AND ANALYSIS OF HYDROGEN TRANSPORT

The interaction [54-58] between solute hydrogen atoms and an applied stress field results from the hydrogen induced volume [59] and local moduli changes [60, 61] that accompany the introduction of the solute hydrogen in the lattice [26, 62]. In regions of tensile hydrostatic stress and softened elastic moduli [25], interstitial hydrogen has a lower chemical potential [63, 64]. As a consequence, diffusion

through normal interstitial lattice sites (NILS) is generated toward these regions tending to eliminate the gradients of the chemical potential. Regions with compressive hydrostatic stress or hardened elastic moduli are depleted [25]. This discussion pertains to situations of hydrogen transport through normal interstitial lattice site diffusion. Hydrogen transport by dislocations moving toward the crack tip may also be important [65]. However, this is an unresolved issue as of yet, since there may be dislocations from internal sources that move away from the tip, thus canceling the effect of those dislocations moving toward the tip. In general though, recent experimental observations do not support the dislocation transport model [66, 67].

Transported hydrogen through NILS diffusion can accumulate at various microstructural heterogeneities such as dislocations, grain boundaries, inclusions, voids, surfaces and impurity atoms described as traps [68-70]. It has been established that trapping is very important part of hydrogen embrittlement and its significance lies behind the embrittling mechanisms [7, 70-77]. However, characterization of the trap type, density, (the number per unit volume), binding energy and occupancy is a difficult problem and much research has been carried out in this direction [75, 78, 79]. Oriani [80] analyzing experimental data for annealed iron concluded that interfaces and microcracks were involved in trapping. Kumnick and Johnson [79] estimated a trap density of 2.77×10^{22} traps/m^3 in iron at deformation levels by rolling of 40% and concluded that this density is not likely to be associated with long range elastic stress fields of dislocations. In a later work, Kumnick and Johnson [81] calculated the trap binding energy in pure iron equal to 60kJ/mole independent of temperature and amount of plastic deformation. Their measured trap densities ranged from 10^{20} traps/m^3 for annealed iron to 10^{23} for heavily deformed iron which were approximately two orders of magnitude smaller than the trap densities at dislocations. Hence, Kumnick and Johnson [81] concluded that traps were

associated with the imperfection structure, dislocations and point defect aggregates or dislocation debris. Commenting on the results of Kumnick and Johnson [81], Johnson and Lin [82] explained that indeed a high binding energy and a low trapping density calculated by Kumnick and Johnson [81] provide the best fit of the analytical results. Later Hirth [7] pointed out that a binding energy value of the order of 60kJ/mole could well correspond to trap sites of the standard mixed or screw dislocation cores.

Studying hydrogen transport in the alloy X-750, Lufrano *et al.* [53] considered that the hydrogen trap sites are associated with dislocations in the deforming metal [83, 84]. Assuming one trap site per atomic plane threaded by a dislocation [83, 85, 86], one finds that the trap site density in traps per cubic meter is given by

$$N_T = \sqrt{2}\,\rho/a, \qquad (1)$$

where ρ is the dislocation density and a is the lattice parameter. This assumption is consistent with the experimental work of Thomas [83] in which the best fit to the experimental data was obtained with a trapping radius of only 1 to 2 atomic spacings. Equation (1) can be used to determine the trap site density once the dislocation density is known as a function of a measure of the plastic deformation, e.g., the equivalent plastic strain ε^p [53]. On the other hand, if one considers that hydrogen is trapped at the octahedral sites on the interface of the γ' precipitates [87], a density of 6.0×10^{26} sites per cubic meter and a binding energy of 15.1 kJ/mole are calculated. However, it should be pointed out that a value of 31 kJ/mole for the trapping binding energy has also been reported in the literature for the alloy X-750 [88].

Neglecting trapping at microstructural defects, Van Leeuwen [89] and Hippsley and Briant [90] calculated the solute hydrogen distribution at a crack tip in an isotropic linearly elastic solid under non-steady state conditions of hydrogen transport. Similar calculations of hydrogen atmospheres at a crack tip in

equilibrium with local stresses were done by Liu [91] in an isotropic linearly elastic material and by Tong-Yi *et al.* [92, 93] in single crystals of elastically anisotropic iron. One dimensional hydrogen transport at a crack tip and the associated crack propagation in an elastic material was studied by Unger [94]. Calculations on NILS populations at a crack tip in equilibrium with local stress were recently carried out by Lufrano and Sofronis [95] in the absence of trapping. In this work the effects of hydrogen induced volume change and modulus softening on the standard crack tip singular elastic solution were investigated.

The effect of trapping on hydrogen transport was first formally modeled by McNabb and Foster [96]. Their analysis is based on probabilistic considerations and places no constraint on the trapping mechanism thus being of very general applicability. However this feature constitutes a source of indefiniteness because the parameters are difficult to measure. Another approach on modeling the trapping effect is that taken by Oriani [80]. Oriani assumed that hydrogen can reside in the interior of the materials either at normal interstitial lattice sites or at lattice imperfections-trapping sites. Then he postulated that at any stage of hydrogen diffusion, the hydrogen populations in reversible traps [7, 70, 74-76, 78, 97], and those in NILS are in local equilibrium. This equilibrium argument is realistic when the lattice diffusion relaxation times are relatively long compared to the time required to replenish or deplete the traps. Oriani concluded that at temperatures around 300K all systems of interest meet the condition for equilibrium because their binding energies are less than a critical binding energy which he identified to be 67kJ/mole. Pressouyre and Bernstein [98] deployed trapping analysis to study hydrogen induced cracking in iron titanium alloys and computed hydrogen populations based on Oriani's theory. It is worth mentioning that most of the numerical solutions to the hydrogen diffusion equation accounting for trapping [99-104] are based on the McNabb and Foster formalism [96], and they do not account for the interactions

between hydrogen concentration, plastic straining and stress. However, notable exceptions are the work of Ellebrock *et al.* [105] and Allen-Booth *et al.* [106].

Coupling of nonlinear diffusion phenomena with elastoplastic deformation was first attempted by Kitagawa and Kojima [107]. Sofronis and McMeeking [108] analyzed transient diffusion of hydrogen and hydrogen trapping at microstructural defects in iron and steel in the area around a blunting crack tip. The diffusion model accounted for drift due to hydrostatic stress and trapping generated by plastic deformation. Modeling the interaction of hydrogen with local elastoplasticity at cracked and rounded— notched geometries, Lufrano and Sofronis [52] extended the model of Sofronis and McMeeking by including the effect of hydrogen induced dilatation on the material constitutive law. In systems with large hydrogen solubility (e.g. niobium), the dilatational effect of hydrogen becomes important at high hydrogen concentrations as it affects both the stress relaxation and the diffusion paths. Krom [109] modified the model of Sofronis and McMeeking by introducing in the diffusion equation a strain rate factor to accurately account for the hydrogen balance in NILS and trapping sites. This strain rate factor is particularly important in transient calculations of hydrogen at high strain rates. Sun et al. [110] found experimentally that the distribution of dissolved hydrogen ahead of a crack tip in a nickel single crystal under load exhibited two peaks that were correlated with the maxima in the plastic strain and the hydrostatic stress.

3. A HYDROGEN TRANSPORT MODEL IN A SOLID STRAINED ELASTOPLASTICALLY

Following Johnson and Lin [82] and Sofronis and McMeeking [108], one can assume that hydrogen resides either at normal interstitial sites or reversible trapping sites generated by plastic deformation. The two populations are always in

equilibrium according to Oriani's theory [80], such that

$$\frac{\theta_T}{1-\theta_T} = \frac{\theta_L}{1-\theta_L} K \tag{2}$$

where θ_L denotes the occupancy of the NILS, θ_T denotes the occupancy of the trapping sites,

$$K = \exp\left(W_B / RT\right) \tag{3}$$

represents the equilibrium constant, W_B is the trap binding energy, R is the gas constant equal to $8.31\,\mathrm{J\,mole^{-1}\,K^{-1}}$ and T is the absolute temperature. The hydrogen concentration per unit volume in trapping sites, C_T, can be phrased as

$$C_T = \theta_T \alpha N_T, \tag{4}$$

where α denotes the number of sites per trap and N_T, which is a function of the local effective plastic strain, i.e., $N_T = N_T\left(\varepsilon^p\right)$, denotes the trap density measured in number of traps per unit volume. The hydrogen concentration in NILS, C_L, can be stated as

$$C_L = \theta_L \beta N_L, \tag{5}$$

where β denotes the number of NILS per solvent atom and N_L denotes the number of solvent lattice atoms per unit lattice volume. If the available number of trapping sites per unit volume, αN_T, is small compared with the available NILS per unit volume, βN_L, then

$$N_L = N_A / V_M, \tag{6}$$

where $N_A = 6.0232 \times 10^{23}$ atoms per mole is Avogadro's number and V_M is the molar volume of the host lattice measured in units of volume per lattice mole.

Hydrogen conservation in any arbitrary material volume combined with Eqs. (2) through (5) yields the governing equation for transient hydrogen diffusion accounting for trapping and hydrostatic drift as [82, 108, 109]

$$\frac{D}{D_{eff}}\frac{dC_L}{dt} = DC_{L,ii} - \left(\frac{DV_H C_L}{3RT}\sigma_{kk,i}\right)_{,i} - \alpha\theta_T \frac{\partial N_T}{\partial \varepsilon^p}\frac{d\varepsilon^p}{dt}, \tag{7}$$

where $(\,)_{,i} = \partial(\,)/\partial x_i$, d/dt is the time derivative, D is the hydrogen diffusion constant through NILS, D_{eff} is an effective diffusion constant given by

$$D_{eff} = D/(1+\partial C_T/\partial C_L), \tag{8}$$

V_H is the partial molar volume of hydrogen in solid solution, σ_{ij} is the Cauchy stress, and the standard summation convention over the range is implied for a repeated index. The last term in the right hand side of Eq. (7) is the strain rate factor of Krom [109]. It is implicit in the Oriani's model that trap filling kinetics is very rapid. Consequently the effective diffusion constant is less than the normal NILS diffusion constant as long as the traps are not saturated or as plastic straining continues and new traps are created. Another important observation is that NILS hydrogen populations can achieve equilibrium with local stress only when plastic straining terminates and new traps are no longer created. Clearly, Eq. (7) demonstrates that the calculation of the hydrogen distribution within a solid is coupled to the fields of the hydrostatic stress and effective plastic strain.

4. ELASTOPLASTIC DEFORMATION IN THE PRESENCE OF HYDROGEN

The hydrogen effect on dislocation behavior [25, 40] is ignored and the flow stress is assumed independent of hydrogen concentration. However, the hydrogen induced lattice deformation is modeled through the dilatational distortion that accompanies the introduction of the hydrogen solutes into the lattice. Thus, the material is considered to harden isotropically under plastic straining, and flow according to von-Mises J_2 flow theory. In the case of finite deformations, the associated flow law is given by the classical Prandtl-Reuss equations [111]

appropriately modified to account for the hydrogen induced dilatational strain:

$$\overset{\nabla}{\sigma}_{ij} = 2G\left[\delta_{ik}\delta_{jl} + \frac{\nu}{1-2\nu}\delta_{ij}\delta_{kl} - \frac{3}{2}\frac{\sigma'_{ij}\sigma'_{kl}}{\left(\frac{h}{3G}+1\right)\sigma_e^2}\right]\left(D_{kl} - D^t_{kl}\right) \tag{9}$$

for plastic loading and

$$\overset{\nabla}{\sigma}_{ij} = 2G\left(\delta_{ik}\delta_{jl} + \frac{\nu}{1-2\nu}\delta_{ij}\delta_{kl}\right)\left(D_{kl} - D^t_{kl}\right) \tag{10}$$

for elastic loading or any unloading, where D_{ij} is the deformation rate tensor and equals the symmetric part of the velocity gradient in spatial coordinates, δ_{ij} is the Kronecker delta, the superposed ∇ denotes the Jaumann or corrotational stress rate (which exhibits proper material invariance for rigid spin), $\sigma'_{ij} = \sigma_{ij} - \sigma_{kk}\delta_{ij}/3$ is the deviatoric stress, $\sigma_e^2 = 3\sigma'_{ij}\sigma'_{ij}/2$ is the equivalent stress, G and ν are the shear modulus and Poisson's ratio respectively, and $h = d\sigma_e/d\varepsilon^p$ is the slope of the uniaxial Cauchy stress versus logarithmic plastic strain, ε^p. In multiaxial deformation ε^p is defined as $\varepsilon^p = \int\sqrt{2D^p_{ij}D^p_{ij}/3}\,dt$, where the deformation rate is expressed as $D_{ij} = D^e_{ij} + D^p_{ij} + D^t_{ij}$ with D^e_{ij} denoting the elastic part, D^p_{ij} the plastic part, and D^t_{ij} the part due to lattice straining by the solute hydrogen. The hydrogen induced deformation rate D^t_{ij} is purely dilatational [59] and, in the context of the large strain formulation, is phrased as

$$D^t_{ij} = \frac{d}{dt}\left\{\ln\left[1 + \frac{(c-c_0)\Delta v}{3\Omega}\right]\right\}\delta_{ij}, \tag{11}$$

where c is total hydrogen concentration (in NILS and trapping sites) measured in hydrogen atoms per solvent atom, c_0 is the initial hydrogen concentration in the absence of any straining, Δv is the volume change per atom of hydrogen introduced into solution that is directly related to the partial molar volume of hydrogen $V_H = \Delta v N_A$ in solution, and Ω is the mean atomic volume of the host metal atom. Note that for small changes of concentration, Equation (11) yields the infinitesimal

strain rate as $\dot{\varepsilon}^t_{ij} = (\dot{c}\Delta v/3\Omega)\delta_{ij}$, where $\dot{c}$ is the time rate of change of concentration.

Lufrano *et al.* [18] demonstrated that in high solubility systems (e.g. niobium) and at relatively high initial concentrations (e.g. 0.3 atoms of hydrogen per metal atom), the stress induced enhancement in the local hydrogen concentration is large enough to cause stress relaxation in front of a crack tip by as much as 20%. They concluded that the hydrogen induced dilatation strain has no effect on the material constitutive only when the initial hydrogen concentration is small, that is, approximately less than 0.01 hydrogen atoms per metal atom.

The governing equations for rate equilibrium accounting for changes of the deformed volume of the material are cited by McMeeking and Rice [111] as

$$\int_V \left(\overset{\nabla}{\sigma}_{ij} + D_{kk}\sigma_{ij} \right) \delta D_{ij} dV - \int_V \tfrac{1}{2}\sigma_{ij}\delta\left(2D_{ik}D_{kj} - v_{k,i}v_{k,j}\right) dV = \int_S \dot{T}_i \delta v_i dS + \int_V \dot{b}_i \delta v_i dV \qquad (12)$$

where V is the volume of the material in the current configuration bounded by the surface S, T_i is the traction which is specified on the part S_T of the surface where tractions are prescribed, b_i is the body force per unit volume in the reference configuration, v_i is the velocity, and δ indicates an arbitrary virtual variation of the quantity it precedes. Note that both $\dot{T}_i$ and $\dot{b}_i$ are nominal rates of change [111]. Any virtual variation of the velocity is constrained to vanish on the part $S - S_T$ of the surface where velocities are prescribed.

It is evident from Eqs. (7-12) that the hydrogen diffusion initial boundary value problem and the elastic-plastic boundary problem are fully coupled. Therefore the problem of calculating the velocity field and the local distribution of hydrogen is coupled in a non-linear sense and the solution procedure involves iteration [25, 52, 53, 108]. The finite element procedures for the solution of the coupled problems are outlined in the work by Sofronis and McMeeking [108], Lufrano *et al.* [53] and Krom [109]. The formulation of Govindarajan and Aravas

[112] for large strain plasticity was adopted to ensure zero lattice strain during large rigid body rotation. Incompressibility of the plastic deformation was enforced by the method of Nagtegaal *et al.* [113].

5. NUMERICAL RESULTS

In this section solutions to the initial boundary value problem of transient hydrogen diffusion coupled with material elastoplasticity are presented: (a) in the neighborhood of a blunting crack tip under small scale yielding conditions; and (b) in a four-point rounded-notch bend specimen. In both cases plane strain conditions were assumed and the system's temperature was 300K. The materials used in the simulations were impure iron/low strength steel, high strength steel, and niobium as these systems suffer from embrittlement at room temperature and experimental data are readily available [7, 51, 59, 60, 108].

Environmental embrittlement conditions were simulated by assuming that the specimen is under a uniform initial NILS hydrogen concentration, $C_L = C_0$. The trapping site concentrations C_T follow from the NILS populations through Eq. (2). The crack or notch free surface was assumed "open" to allow equilibration with the hydrogen gas, and therefore a constant concentration boundary condition , $C_L = C_0$, was enforced on the boundary of the domain at all times. In the case of internal embrittlement, at time zero hydrogen is in NILS and trapping sites, the two populations $C_L = C_0$ and C_T being in equilibrium as Eq. (2) dictates. All external surfaces including those of the crack or the notch were assumed to be insulated (zero hydrogen flux). Such a specimen is obtained via cathodic or thermal charging followed by insulation of its surfaces to preclude hydrogen loss.

5.1. Blunting crack

The boundary layer approach of small scale yielding (see Fig. 1) under mode I (tensile) opening was used in the calculations. The finite geometry material was replaced by an infinite body with a semi-infinite crack and the asymptotic displacement boundary conditions of the Irwin [114] singular linear elastic field were imposed at the circular boundary at a distance $L = 15\text{cm}$ from the tip. These displacements were applied incrementally at a constant stress intensity factor rate $\dot{K}_I$ during a loading time t_l, at the end of which the final value of K_I was K_A. At times greater than t_l the displacements were kept constant while hydrogen diffusion was allowed to continue. The ratio L/b_0, where b_0 is the initial crack opening displacement, was taken equal to 30,000. The finite element mesh is described in the work of Sofronis and McMeeking [108].

5.1.1. Low strength steel

The uniaxial stress-strain law was given by a power-law hardening relationship of the form $(\sigma_e/\sigma_0)^{1/N} = (\sigma_e/\sigma_0) + (3G/\sigma_0)\varepsilon^p$, where the yield stress σ_0 was equal to 250MPa, the work hardening exponent was 0.2, and G is the shear modulus. Poisson's ratio ν was 0.3 and Young's modulus E was 207GPa. At the end of loading, i.e., at time $t = t_l$, the final value of the stress intensity factor was $K_A = 89.7\text{MPa}\sqrt{\text{m}}$ and the corresponding crack opening displacement b was equal to $5b_0$.

The lattice diffusion constant of hydrogen at 300K was $D = 1.27\times10^{-8}\,\text{m}^2/\text{s}$ [115]. The interstitial hydrogen expands the lattice isotropically [58] and its partial molar volume in solution was $2.0\times10^{-6}\,\text{m}^3/\text{mole}$ [7]. The molar volume of iron was $7.116\times10^{-6}\,\text{m}^3/\text{mole}$ and hence $N_L = 8.46\times10^{28}$ solvent lattice atoms per m^3. Uniform hydrogen concentration in the unstressed lattice, $C_0 = 2.084\times10^{21}$ atoms per

m^3 (2.46×10^{-8} atoms per solvent atom) in equilibrium with gas at one atmosphere pressure was used as initial condition. The parameter α was taken equal to 1. The parameter β was set equal to 1 and this corresponds to a maximum NILS concentration of 1 hydrogen atom per solvent lattice atom. The trap density N_T was assumed to increase with plastic straining, ε^p, according to the experimental results of Kumnick and Johnson [81] as shown in Fig. 2. and the trap binding energy was 60kJ/mole. It should be pointed out that the function $N_T(\varepsilon^p)$ interpolating the experimental data in Fig. 2 increases monotonically with ε^p and no trapping site saturation level exists, as was the case in the Sofronis and McMeeking [108] calculations.

(i) *Concentration boundary conditions.* Figures 3 through 5 show the distribution of field parameters on the axis of symmetry ($\theta=0$) ahead of the crack tip at the end of loading ($b=5b_0$) at times $t_l=1.3$, 13, and 130s.

In Fig. 3 the equivalent plastic strain ε^p and the normalized hydrogen distribution at trapping sites C_T/C_0 prevailing at the end of loading are plotted against the distance R from the notch root in the undeformed configuration. Distance R is normalized by the current crack opening displacement b. Also shown is the concentration C_T at steady state after approximately 3 h have elapsed and after the loading has terminated. The site of accumulation of trapped hydrogen is near the crack surface and the profile of the concentration C_T follows closely that of the plastic strain (Fig. 3). This is because the trap density increases monotonically with plastic strain as shown in Fig. 2. At the crack surface, where the effective plastic strain is maximum and equal to 1.6, concentration C_T assumes its maximum value which is equal to 91 times as large as the initial concentration C_0. It can be seen that the loading rate has no effect on the trapped hydrogen populations. Diffusion of hydrogen through NILS delivers hydrogen to trapping sites at a rate faster than the

rate at which traps are generated by plastic straining. As a result, the trapping sites are always saturated due to the high binding energy, with the exception of the traps in a small segment of size 0.3b centered at $R/b = 0.7$ from the tip when the rate of loading is very fast, ($t_l = 1.3$s). The trap occupancy in that segment though is not less than 86%. Therefore, once loading has ceased and traps are no longer created by plastic straining, there is almost no change in the trapped concentration. As a result, trapped hydrogen concentrations C_T reach their steady state values (saturated traps) upon load termination.

In Fig. 4 the normalized hydrostatic stress $\sigma_{kk}/3\sigma_0$ and the normalized concentration C_L/C_0 in NILS are plotted against distance R/b for the three loading courses. While the trapped hydrogen concentration profiles are loading rate independent, the accumulation of hydrogen in NILS decreases with increasing loading rate. At slow strain rates ($t_l = 13{,}130$s), the distribution of concentration C_L varies with distance from the notch root in accordance with the hydrostatic stress and it attains its maximum at $r/b = 1.53$. However, at higher strain rates ($t_l = 1.3$s), a trough is established in the NILS population profile somewhere between the notch surface and the site of the hydrostatic stress peak location. Trap generation rate close to the notch surface increases with strain rate causing more demand for hydrogen at the crack tip. On the other hand, hydrostatic stress gradients pull hydrogen away from the tip toward the hydrostatic stress peak at $r/b = 1.53$. In addition, the crack tip concentration C_L is kept constant at the value of C_0 at all times. The competition between these three processes dictates the shape of the NILS concentration profiles. Thus, at high strain rates the trap generation rate is "ahead" of hydrogen diffusion. As a result, hydrogen in the region $0 \le R/b \le 1.53$ is depleted from NILS sites to satisfy the elevated demands for hydrogen in the trapping sites close to the notch surface and the hydrostatic stress peak location. As a consequence, a trough is established in the NILS hydrogen distribution somewhere in between the notch

surface and the site of the hydrostatic stress peak. It should be noted here that such a trough was not observed in the calculations of Sofronis and McMeeking [108] and Lufrano and Sofronis [52] at high strain rates because of the omission of the strain rate term [109] from the diffusion equation (7). In addition, the crack tip concentration C_L is maintained at the constant value C_0 by hydrogen ingress through the crack surface. In contrast, at slow strain rates the demand for trapping hydrogen is less severe and traps are saturated by the end of loading. Hence, diffusion through NILS and the ingress of hydrogen through the crack surface can supply hydrogen to the trapping sites close to the crack tip and the hydrostatic stress peak location without the establishment of a trough.

Unlike the trapping site concentrations, the NILS concentrations by the end of loading are away from their steady state values (see Fig. 4). Obviously the most dramatic departure from steady state occurs with loading at high strain rates. As a result, the total hydrogen concentration profiles $C_L + C_T$, shown plotted against R/b on Fig. 5, are also away from steady state by the end of loading. It is notable that even at steady state, NILS concentration C_L is only mildly elevated at the peak of the hydrostatic stress location at some distance from the tip. The maximum steady state NILS concentration C_L is only 1.82 as large as C_0 at a distance $R = 1.53b$ from the tip. Lastly, after the chemical potential of hydrogen in the area ahead of the crack tip is neutralized, that is, at steady state, the constant concentration boundary condition at the tip is maintained by an egress of hydrogen from the specimen through the crack surface.

(ii) *Zero flux boundary conditions.* For the three loading courses, the normalized hydrostatic stress $\sigma_{kk}/3\sigma_0$ and the hydrogen concentration C_L/C_0, and the normalized total concentration $(C_L + C_T)/C_0$ are plotted respectively in Figs. 6 and 7 on the axis of symmetry ($\theta = 0$) ahead of the crack tip at the end of loading

($b = 5b_0$). Also shown are the corresponding concentrations at equilibrium with local stress after approximately 3 h have elapsed and after the loading has terminated.

The transient hydrogen concentrations during straining are now somewhat smaller than in the case of constant concentration boundary conditions. With zero flux boundary conditions, the demand for trap filling hydrogen at the crack surface and for hydrogen to be delivered to the NILS at the high hydrostatic stress region is met only with hydrogen drawn by NILS diffusion toward the crack tip from the bulk of the specimen remote from the tip. In other words the additional supply of hydrogen through the crack surface (which was the case at constant concentration boundary conditions) is absent in the insulated specimen. Hence, the lattice sites in the insulated specimen are depleted more since less NILS hydrogen is available to be distributed according to the concentration gradient and hydrostatic stress induced diffusion. Also, due to the lack of this additional supply of hydrogen no trough is observed in the transient NILS population profile at high strain rates. In fact when the loading is fast ($t_l = 1.3,13\text{s}$), the NILS at the crack tip region in the insulated specimen are severely depleted of hydrogen since less hydrogen is now available to meet the demands of the trapping sites. It is notable that a strain rate ($t_l = 13\text{s}$) which is low for a specimen with concentration boundary conditions (Fig. 4), may be high (Fig. 6) in the case of an insulated specimen.

In contrast with the transient NILS concentrations, after the loading has terminated and the NILS hydrogen population relaxes to its equilibrium distribution, the values of C_L in the insulated specimen are larger than those in the constant concentration boundary condition specimen. This is due to the constant egress of hydrogen from the specimen through the notch root in the latter case in order for the concentration to be kept at the constant value of C_0. On the other

hand, the equilibrium NILS concentration at the crack tip in the former case is about 1.5 times as large as C_0 . As in the case of concentration boundary conditions, the maximum equilibrium value of C_L is also attained at $R/b = 1.53$ from the tip and the corresponding value is 1.98 times the initial concentration C_0.

Due to the high binding energy, at slow and moderate strain rates ($t_l = 130, 13\text{s}$), the trapping sites are saturated during loading. Accordingly, there is no variation to the trapping concentration after straining. Thus, any changes in total concentration of hydrogen is due to the variations in the NILS concentration. Since the magnitude of NILS populations is much smaller than that of the trapped populations, the profile of the total concentration of hydrogen $C_L + C_T$ (Fig. 7) is almost the same as that for constant concentration boundary condition case (Fig. 5), in which traps were also saturated during straining.

At high strain rates ($t_l = 1.3\text{s}$), lattice diffusion fails to saturate the traps during loading. Trap occupancy in the region $0 \le R/b \le 1$ is less than 55%. Consequently, as shown in Fig. 7, the total concentration $C_L + C_T$ at the tip of the notch is approximately equal to the half of its corresponding steady state value. However, as in the case at slower strain rates, the trapped hydrogen concentrations continue to dominate the total concentration profile (Fig. 7) since the NILS concentrations are of much smaller magnitude. Eventually at steady state, traps become saturated even at high strain rates. As a result, the distribution of hydrogen after long time from the termination of loading is independent of boundary conditions (Figs. 5, 7). As in the case of constant concentration boundary condition, the maximum equilibrium value of C_T at the notch root is 91 times the initial concentration C_0 (Fig. 7).

5.1.2. High strength steel

This material had a yield stress σ_0 of 1200 MPa and work hardening exponent N equal to 0.2. The rest of the material and hydrogen related constants were assumed exactly the same as those for low strength steel. The loading was imposed at a constant displacement rate and the load times were $t_l = 0.4$, 4, and 40 s. The final value of the stress intensity factor was $K_A = 132\,\text{MPa}\sqrt{\text{m}}$, and the corresponding crack opening displacement b was equal to $3.5b_0$.

In Figs. 8 and 9 the normalized concentration C_L/C_0 and hydrostatic stress $\sigma_{kk}/3\sigma_0$ are plotted against distance R/b on the axis of symmetry ($\theta = 0$) ahead of the crack tip respectively for constant concentration and zero flux boundary conditions at the end of loading ($b = 3.5b_0$) for the three loading courses. In Figs. 10 and 11 the corresponding normalized total concentration $(C_L + C_T)/C_0$ is plotted against distance R/b respectively for the two cases of boundary conditions. Also shown plotted respectively in Figs. 8 and 10 are the steady state concentrations C_L/C_0 and $(C_L + C_T)/C_0$ under concentration boundary conditions achieved after approximately 500 s. Similarly, the equilibrium concentrations C_L/C_0 and $(C_L + C_T)/C_0$ for zero flux boundary conditions achieved after approximately 500 s are also shown respectively in Figs. 9 and 11. Again, the effects of hydrostatic stress, plastic strain, strain rate and boundary condition on the concentration profiles are qualitatively the same as in the case of mild strength steel.

The maximum NILS concentrations C_L for concentration and flux boundary conditions are attained for both cases at distance $R/b = 1.6$ from the notch surface. The corresponding maximum values of C_L are 9 and 15 times the initial concentration C_0. These values are much higher than respective values of 1.82 and 1.98 in low strength steel; and this derives from the fact that at the end of loading the maximum hydrostatic stress in the high strength steel is $\sigma_{kk} = 12600\,\text{MPa}$ (Fig. 4)

whereas in the low strength steel $\sigma_{kk} = 3575\,\text{MPa}$ (Fig. 8). Figures 10 and 11 indicate that the hydrostatic stress effect beyond the high trap density region at the notch surface is drawing hydrogen toward the site of the hydrostatic stress peak in large quantities. At that location, the plastic strain and therefore the density of traps is low. As a result, most of the hydrogen there resides in NILS since the demand for trap filling hydrogen is zero (due to saturation at all times). As a consequence, a local minimum is observed in the total hydrogen concentration profile in the segment $0 \le R/b \le 2$ (Figs. 10, 11) when the local chemical potential gradients are neutralized with time. It is notable that no such local minimum was observed in the case of mild steel (Figs. 5 and 7). Apparently, the hydrostatic stress at the peak location in the low strength material is not sufficiently high to attract hydrogen there in large quantities.

Again as in the case of low strength steel, the total equilibrium concentration of hydrogen $C_L + C_T$ under zero flux boundary conditions (see Fig. 10) is the same as the steady state profile for constant concentration boundary conditions (see Fig. 11).

5.1.3. Niobium

BCC niobium (yield stress, $\sigma_0 = 250\,MPa$, power law hardening exponent, $N = 0.2$) is a system that allows for high hydrogen solubilities in contrast to iron. As in the case of steels, the parameters α and β were chosen equal to 1. The partial molar volume of hydrogen in solution with the metal was $V_H = 1.88\,\text{cm}^3/\text{mole}$ and the expansion of the lattice due to hydrogen was purely dilatational [59]. The molar volume of niobium was $10.852 \times 10^{-6}\,\text{m}^3/\text{mole}$ and the NILS diffusion constant at 300K was $D = 8.3 \times 10^{-10}\,\text{m}^2/\text{s}$ [115]. The trap binding energy was taken 29.2kJ/mole, as has been calculated by Baker and Birnbaum [116]. Since no experimental data for trap populations are available, the trap density was quantified through the

dislocation based model of Eq. (1). The dislocation density ρ, measured in dislocation line length per cubic meter, was considered to vary linearly with plastic strain [117], namely $\rho = \rho_0 + \gamma\varepsilon^p$ for $\varepsilon^p < 0.5$ and $\rho = 10^{16}$ for $\varepsilon^p \geq 0.5$, where $\rho_0 = 10^{10}$ dislocation lines per cubic meter denotes the dislocation density for the annealed material and $\gamma = 2.0 \times 10^{16}$ lines/m^2. Given the lattice parameter $a = 3.3 \times 10^{-10}$ m, the maximum number of trapping sites per cubic meter, $\alpha N_T = 4.28 \times 10^{25}$ traps/m^3, was much smaller than the number of the available NILS, $N_L = 5.55 \times 10^{28}$ solvent lattice atoms per m^3. The Poisson's ratio was 0.39 and Young's modulus was 113 GPa. The crack was loaded at a constant displacement rate during a loading time t_l, at the end of which the final load phrased in terms of the applied stress intensity factor was $K_A = 40\,\text{MPa}\sqrt{\text{m}}$. At times greater than t_l the load was kept constant at $K_A = 40\,\text{MPa}\sqrt{\text{m}}$.

Figures 12 through 14 show the hydrogen concentrations C_L, C_T and the sum $C_L + C_T$ normalized by the initial concentration C_0 plotted against distance R/b on the axis of symmetry ($\theta = 0$) ahead of the crack tip at the end of loading ($t = t_l = 120$ s) when $b = 2.6 b_0$. The hydrogen concentration profiles are also plotted after 120 minutes when hydrogen relaxes to the steady state concentration values. In addition, in Figs. 12 through 14 constant concentration C_0 was prescribed as boundary condition over the entire boundary of the specimen. It was found that the results for zero flux boundary condition were not qualitatively different and this is why they are not reported. Figure 12 shows that for a normalized initial concentration C_L^0/N_L of 10^{-4} hydrogen atoms per niobium atom, the total concentration is dominated by trapped hydrogen populations and the maximum value is attained close to the crack tip. At this low level of initial lattice concentration, traps are occupied at 92% before straining begins, and this is the reason that no significant change in the trap concentration is observed. After the loading terminates, the changes in the NILS concentration C_L are not significant, an

indication that the strain rate is sufficiently slow so that near equilibrium conditions prevail during straining. When the nominal concentration is higher, i.e. $C_L^0/N_L = 10^{-3}$, the trap and NILS populations are of the same magnitude at the tip, whereas at distances R/b greater than approximately 0.1 the magnitude of C_L is about 10 times as that of C_T due to the low plastic strains. As a consequence, a local minimum is observed in the total hydrogen concentration profile in the segment $0 < R/b < 2$ (see Fig. 13). Again no dramatic changes in the transient concentrations are observed and the trap occupancy during straining is always 99%. At an even higher initial concentration, $C_L^0/N_L = 10^{-2}$, the NILS concentrations are much greater than the trap concentrations and the hydrostatic stress dominates the hydrogen distribution at all times (see Fig. 14).

Lastly, the maximum total hydrogen concentration in the neighborhood of the crack tip is less than 1.9 times the initial concentration C_0 for zero flux boundary conditions.

5.2. *Rounded-notch specimen*

The four-point bend-specimen of Griffiths and Owen [118] shown in Fig. 15 was employed in the analysis. Uniform initial NILS concentration of 2.46×10^{-8} atoms per solvent atom was used throughout as an initial condition. The outer surface of the specimen was modeled either as impermeable or was held at constant NILS concentration equal to the initial concentration during straining. The specimen was loaded in plane strain by prescribing displacement increments Δu_1 at points A and B (Fig. 15). The loading was performed at constant displacement rates $\Delta u_1/\Delta t$ of 0.002mm/s for low strength steel and 0.1mm/s for high strength steel until loading was completed ($t = t_l$), at which time the loading displacements at points A and B were held constant and hydrogen diffusion continued under fixed

held displacements. The extent of deformation and loading in the specimen was measured in terms of a nominal stress defined as $\sigma_{nom} = 6M/wa^2$, where $M = Fd$ is the bending moment due to the reaction forces F at points C and D, d is the bending moment arm, a is the unnotched ligament and w is the specimen thickness. The nominal stress σ_{nom} denotes the maximum bending stress in an straight beam of height a. In the following the hydrogen concentration profiles are plotted vs normalized distance R/r_0 along the axis of symmetry directly beneath the notch, where R is measured from the tip of the notch, and r_0 is the undeformed notch root radius.

5.2.1. Low strength steel

Three loading courses were applied respectively with load times t_l=17, 40, and 107s. At the end of loading, the corresponding normalized nominal stresses σ_{nom}/σ_0 were 1.0, 2.0 and 3.0; and the corresponding plastic strains at the root of the notch were 0.5, 2.0 and 8.0%. The peak hydrostatic stresses $\sigma_{kk}/3\sigma_0$ were respectively 1.3, 2.0 and 2.7, and they were achieved at a distance $R/r_0 = 0.8$, 1.2, and 1.7 from the tip of the notch. Plastic straining at the notch root commences when $\sigma_{nom}/\sigma_0 = 0.32$, whereas on the other side of the specimen opposite the notch root, it commences at $\sigma_{nom}/\sigma_0 = 1.42$. Obviously, yielding is contained for the loading course with maximum $\sigma_{nom}/\sigma_0 = 1.0$ ($t_l = 17$s), and still is not fully spread throughout the uncracked ligament even in the case of the course with maximum $\sigma_{nom}/\sigma_0 = 3.0$ ($t_l = 107$s).

For the three loading courses the normalized hydrogen concentration C_L/C_0, C_T/C_0, and $(C_L + C_T)/C_0$ is plotted respectively in Figs. 16, 17 and 18, at the end of loading for both zero flux and constant concentration boundary conditions. The C_L/C_0 profiles vary with distance from the notch root in accordance with the

hydrostatic stress and the order of magnitude is in accordance with the level of hydrostatic stress elevation. Evidently, the rate at which the loads are applied is small enough for the hydrogen diffusion through NILS to keep up with the demand for trap filling hydrogen. In the case of zero flux boundary condition the NILS concentration is somewhat larger than in the case of constant concentration boundary condition. This is due to the constant egress of hydrogen from the specimen through the notch root in the latter case in order for the concentration to be kept at the constant value of C_0. The C_T/C_0 profiles vary with distance from the notch root in accordance with the equivalent plastic strain. Since the trap binding energy is relatively high and the strain rate is low, the traps always saturate during straining. Only at relatively low plastic strains (less than 0.5%), i.e. for loads such that $\sigma_{nom}/\sigma_0 \leq 1.0$, is the total hydrogen population in the material dominated by the hydrostatic stress effect (see Fig. 18). At high plastic strains, which occur when $\sigma_{nom}/\sigma_0 > 2.0$, the plastic strain effect dominates. It is notable that this behavior is virtually independent of the boundary conditions.

After the loading terminates and traps are no longer created, the trapped hydrogen concentration C_T/C_0 does not vary with time. However, hydrogen diffusion through NILS continues toward the hydrostatic stress peak location and the local NILS concentration profiles continue to change at all locations until the chemical potential gradients of hydrogen are neutralized. The growth of the hydrogen populations and the equilibrium and steady state values are shown in Figs. 19, 20 and 21 for the three different loading cases. For small plastic strains ahead of the notch, $\sigma_{nom}/\sigma_0 \leq 1.0$, the trap concentration is small and the shape of the hydrogen concentration profile depends on the boundary conditions (see Fig. 19). For constant concentration boundary conditions the NILS concentration is necessarily equal to C_0 at the notch tip. However, for zero flux boundary condition the NILS concentration at the notch tip will be larger than C_0 as dictated by the local

hydrostatic stress gradients. Therefore the zero flux boundary conditions yield higher NILS concentration at the hydrostatic stress peak location. Thus regardless of the level of plastic strain the interstitial hydrogen populations in the region from the notch root to the hydrostatic stress peak location are larger in the case of zero flux boundary conditions. On the other hand, since the trapping sites are saturated, there is no variation to the trapping concentration due to boundary conditions. Accordingly the effect of boundary conditions on the total concentration of hydrogen is due to the variations in the NILS concentration. Hence at low plastic strains, $\sigma_{nom}/\sigma_0 \leq 1.0$, where the NILS concentration is dominant the boundary condition affects the total hydrogen concentration close to the surface of the notch (see Fig. 19). Whereas, at high plastic strains, $\sigma_{nom}/\sigma_0 > 2.0$, that is, near general yield where trapping is dominant, the effect of boundary conditions on the total hydrogen concentration close to the notch surface is smaller (see Fig. 21). It is notable that the maximum total hydrogen concentration in all loading cases is less than 3.25 times the initial concentration C_0.

5.2.2. *High strength steel*

Two loading courses with load times t_l=1.65 and 3.8s respectively were simulated. At the end of loading, the corresponding normalized nominal stresses σ_{nom}/σ_0 were 1.0 and 2.0; and the corresponding plastic strains at the root of the notch were 2.4 and 8.8%. The peak hydrostatic stresses $\sigma_{kk}/3\sigma_0$ were respectively 1.3, and 1.94, and they were achieved at a distance $R/r_0 = 0.8$, and 1.3 from the tip of the notch. As in the case of mild steels, plastic straining at the notch root commences when $\sigma_{nom}/\sigma_0 = 0.32$, whereas on the other side of the specimen across from the notch root, it commences at $\sigma_{nom}/\sigma_0 = 1.42$. Hence, when the load time was $t_l = 1.65$s, yielding was contained. In the other case, when $t_l = 3.8$s, general

yielding was not established by the end of loading.

The results shown in Figs. 22 and 23 indicate that in high strength steels the hydrostatic stress dictates the shape of the equilibrium and steady hydrogen concentration profiles at least up to plastic strains equal to 2.4% ($\sigma_{nom}/\sigma_0 = 1.0$) at the notch root (see Fig. 22). It also continues to influence the profiles even at strains as large as 8.8% ($\sigma_{nom}/\sigma_0 = 2.0$) (see Fig. 23). This is due to the large magnitude of the peak hydrostatic stress ($\sigma_{kk}/3 = 1560\,\text{MPa}$) in comparison with the corresponding small hydrostatic stress ($\sigma_{kk}/3 = 325\,\text{MPa}$) in low strength steels under the same normalized nominal stress of 1.0. However, when $\sigma_{nom}/\sigma_0 = 2.0$, the trapping sites close to the surface of the notch begin to strongly compete with the hydrostatic stress peak location for trap filling hydrogen. As a result, a minimum in the total concentration is observed in the region $0 \le R/b \le 2$. Lastly, the maximum total hydrogen concentration for all loading cases studied is less than 5.2 times the initial concentration C_0.

At the end of loading, Figures 22 and 23 show that hydrogen concentrations under constant concentration conditions are larger than those under zero flux boundary conditions, unlike the case of rounded-notch specimen of low strength steel (see Fig 18). The reason is that the traps close to the notch surface are not fully saturated for the high strength steel under zero flux boundary conditions since they compete for hydrogen with the large hydrostatic stress away from the notch root. On the other hand, under constant concentration boundary conditions, the traps are saturated due to the hydrogen ingress through the notch root. When equilibrium or steady state are reached, the traps have saturated and the total hydrogen concentration is larger for flux boundary conditions than for constant concentration boundary conditions. As in the case of low strength steels, hydrogen diffuses out of the specimen in the former case in order for the tip concentration to be kept

constant.

6. DISCUSSION

The results reported in the preceding section indicate that there are two competing mechanisms [52] influencing the distribution of hydrogen near a crack tip or a notch. One is the traps generated by plastic straining (concentration C_T) and the other is the tensile hydrostatic stress (concentration C_L). The site of accumulation of trapped hydrogen is near the crack or notch surface as dictated by plasticity, and the site of accumulation of NILS hydrogen is in the high triaxiality regions at some distance from the crack or notch surface.

It has been demonstrated that in low fugacity systems (e.g., low solubility low and high strength steels) and in situations of severe plastic straining as with blunting crack tips, hydrogen concentrations (transient, equilibrium or steady state) in the region close to the crack surface are always greater than the concentrations at the hydrostatic stress peak location (see Figs. 5, 7, 10, 11), as Sofronis and McMeeking [108] and Lufrano and Sofronis [51] also found. The same is also true in the case of rounded notch specimens of low strength steels provided that large plastic yielding is not confined to the notch root. When the equivalent plastic strain at the tip of the notch is not less than 8.0% (i.e. the case when $\sigma_{nom}/\sigma_0 = 3.0$), the preponderance of the hydrogen resides close to the notch surface (see Figs. 18, 21). However, when the plastic strain at the notch root is very small, namely about 0.5%, the calculations show that hydrogen accumulates at the hydrostatic stress peak location in from the tip (see Fig. 16, 19). In rounded-notch specimens of high strength steel, even though the transient concentration profiles are dominated by the trapped hydrogen close to the notch surface, the hydrostatic stress dictates the shape of the equilibrium or steady state hydrogen concentration distribution even at plastic strains as large as

2.4% (when $\sigma_{nom}/\sigma_0 = 1.0$) (see Figs. 22, 24).

Concerning the results for the effect of the strain rate, at low strain rates hydrogen can diffuse rapidly relative to the rate at which traps are created (See Fig. 4, 6, 8, 9, 12-14, 16, 18). Consequently, traps can be filled readily and the lattice concentration maintained. As a result, the concentration C_L is more pronounced about the hydrostatic stress peak (see Figs. 4, 6, 8, 9, 12-14, 16). At high loading rates, diffusion through NILS is too slow to supply the traps in the high plastic region which exert an attraction for hydrogen. The traps are filled from the lattice nearby, and this has the effect of depleting the lattice and diminishing the relative hydrogen concentration in the high hydrostatic stress region (see Figs. 4, 6, 8, 9). This effect is more pronounced during straining of insulated specimens (see Figs. 4, 6, 8, 9) since trap filling hydrogen is supplied only from the high hydrostatic stress region, whereas for a specimen with constant concentration boundary conditions, hydrogen enters the specimen also through the crack surface. It should be emphasized though, that at blunting crack tips, the maximum NILS concentration is generally negligible compared with the maximum trapping site concentration and so this particular effect of strain rate may be unimportant in processes causing hydrogen failures if it is the trapped hydrogen which is important [108]. On the other hand, at round- notched specimens in which concentrations C_L and C_T are of the same order of magnitude (see Figs. 16, 17, 22, 23), this diffusion related strain rate effect may be important.

In high fugacity systems, (e.g., niobium) the site of accumulation depends strongly on the nominal concentration and the magnitude of the plastic strain. At initial concentrations less or equal than 10^{-4} trapping is dominant and the peak hydrogen concentration occurs at the tip of the blunting crack. However, hydrostatic stress dictates the population distribution even in the neighborhood of a blunting crack tip when the initial hydrogen concentration is high, that is, greater than 10^{-2}

hydrogen atoms per metal atom.

It has been found that in steels and impure irons there is only a small elevation, less than 100 times the initial concentration of hydrogen in equilibrium with hydrogen gas at 1 atm, of the local hydrogen concentration ahead of a notch or a crack tip due to the local trapping and hydrostatic stress effect. Similarly, a mild elevation, less than 2 times the initial concentration of 0.01 hydrogen atoms per metal atoms, of the hydrogen concentration was also the case in the niobium system. The dilatational distortion (cf. Eq. (11)) associated with these concentrations is small compared with the corresponding strain due to the applied loads [18]. Therefore at room temperature and at the initial concentration considered, the effect of hydrogen on stress relaxation is not significant .

The current results can be used to better understand certain aspects of the hydrogen embrittlement problem. The following discussion [52] is general and assumes that no second phase particles or inclusions are necessary for the failure mechanisms to operate. Sofronis and Birnbaum [25] in an effort to identify the underlying principle in the HELP mechanism for hydrogen embrittlement demonstrated that hydrogen trapped at dislocations is responsible for the enhanced dislocation mobility in the presence of hydrogen. Hence, the hydrogen effect will be assumed to be related with the total, NILS and trapping site, populations $C_L + C_T$.

A commonly found assertion in the literature is that a critical hydrogen concentration at some location of the material is needed for the hydrogen effect to initiate. Thus, if a critical concentration alone is the criterion for fracture, one by experimenting with rounded notch bend specimens of low or high strength steels should expect that if fracture occurs at low normalized nominal stresses, ~ 0.1, the failure event should first be observed at the hydrostatic stress peak location. The results with the niobium system can be used to verify this thesis by just changing the nominal concentration in a cracked specimen. At low concentrations the

cracking event should start at the tip whereas at high concentrations the location of the first cracking should be expected to move inside from the tip. Similarly, if a cracked specimen of either low or high strength steel is used and loaded to undergo blunting, the fracture event is to be observed first at the tip of the crack. These conclusions are independent of the mechanism responsible for the hydrogen induced failure. Therefore, one cannot identify the type of the mechanism from the cracking location in experiments with cracked and notched bodies if a critical hydrogen concentration is the local fracture criterion. For instance, the mechanism may be lattice decohesion, and the cracking event in a system like niobium may occur under low hydrogen fugacities at a blunting crack tip where the critical concentration condition is first met and the stress is low. On the other hand, the mechanism of embrittlement may be through hydrogen enhanced localized plasticity and the fracture in rounded-notch specimens of iron and steel may be first triggered at the hydrostatic stress peak location under loads causing no substantial plastic straining at the tip.

If the criterion for fracture requires a critical concentration in combination with a high local stress, say, along the grain boundaries (lattice decohesion) then the experiments on the rounded notch (low or high strength steel) will show cracking in from the tip if fracture occurs at a low nominal normalized stress, ~ 0.1. On the other hand, a blunted crack specimen of low or high strength steel may not be affected by hydrogen due to absence of high local stresses at the crack tip region despite the presence of high hydrogen concentrations there. In fact, in this case cracking may occur somewhere in between the crack tip and the hydrostatic stress peak location where hydrogen concentration is still far above the initial and the local tensile stress is greater than at the tip location. Again as in the case of iron systems, at low nominal concentrations a cracked specimen of niobium may not fail but it will definitely microcrack inside from the tip at high concentrations. The

discussion in this paragraph can also be applied to the case when the role of hydrogen is to promote void nucleation at inclusions through the process of local stress assisted interface decohesion.

If the criterion for fracture requires a critical concentration in combination with local material softening (enhanced dislocation motion) then the fracture event in rounded notched specimens of low or high strength steel may not occur until the loads are raised sufficiently high ($\sigma_{nom}/\sigma_0 \approx 2.0, 3.0$) so that most of the hydrogen is forced to reside close to the highly strained region at the tip where the dislocation density is high. Similarly in a cracked niobium specimen, hydrogen induced cracking may be possible even at low initial concentrations when hydrogen resides mostly close to the tip. These comments also pertain to the case of hydrogen assisted void nucleation at inclusions through local material softening (dislocation pile-ups against the inclusion-matrix interface) and in turn plastic flow localization along the interface.

7. IMPLICATIONS FOR HYDROGEN EMBRITTLEMENT IN STEELS

In the following the numerical results reported in this work on rounded notch 4-point bend specimens will be utilized to address the location of the hydrogen induced crack initiation site in experimental investigations of hydrogen embrittlement in steels. If a critical concentration, $C_L + C_T$, of the hydrogen solute is required for hydrogen embrittlement to occur, the present study can help in rationalizing the location of the first cracking event. The site identification is qualitative in nature given the variability of the model parameters as they apply to a specific steel [65]. For instance, it is not certain whether the Kumnick and Johnson [81] trapping model and the associated binding energy can still be used to the sorts of steels used by other researchers in their experiments. Thus, specific model parameters and pertinent details may first need to be adjusted on a case by case basis

to use the present model to reliably determine the location of the first cracking event due to hydrogen.

Lee *et al.* [120, 121] and Onyewenyi and Hirth [122] carried out experiments on precharged rounded notched bend specimens in spheroidized AISI 1095 steel (yield stress of 380MPa) and spheroidized AISI 1090 steel (yield stress 345) respectively, and identified the role of hydrogen as promoting flow localization (plastic instability) [1, 21, 22, 25] that leads directly to crack initiation at the crack surface. The results were independent of the radius of curvature which shows absence of high triaxiality effect. In the experiments of Lee *et al.* [120, 121], void initiation was observed at strains of 6.0% and hydrogen enhanced the formation of deformation induced void initiation. In the experiments of Onyewenyi and Hirth [122], it was found that at strain of 12.0% cracking was demonstrated to occur at the surface of the notch and to begin to propagate along characteristic slip traces before any significant cracking or void formation occurred in the plastically deformed region beneath the notch root. Based on the present study these are cases in which hydrogen concentration close to the surface of the rounded notch is much larger than the concentration away from the surface.

Lee et al. [122] performed experiments on precharged U-notched specimens of tempered AISI 4340 steel ($\sigma_0 = 1280 MPa$) and found that the notch root strain for crack initiation was at most 1.0%. They also found that MnS inclusions had little role in the fracture process. The results were interpreted to indicate internal crack nucleation at a critical combination of hydrogen concentration and local stress concentration a result which is consistent with the decohesion theory for hydrogen embrittlement first introduced by Troiano and co-workers [26-28] and later elaborated by Oriani and Josephic [29-30], and Gerberich and co-workers [31-32]. Crack initiation occurred in a mode I manner with a subsequent Mode II region connecting the crack to the surface through hydrogen promoted (as the authors

claim) plastic instability along characteristic slip traces. These results pertain to the case of the present calculations in which hydrogen concentration in high strength steels under small strains attains its maximum at the hydrostatic stress peak location.

Investigating the effects of hydrogen on plastic flow and fracture in iron and steel, McMahon and co-workers [124-126, 127-130] found that hydrogen produces brittle fracture by decohesion of grain boundaries already weakened by impurity segregation [131-134]. Takeda and McMahon [124] studied the hydrogen effect through tests at notched four-point bend specimens (of the Griffiths and Owen type [118]) in air and hydrogen using a 5pct Ni quenched and tempered steel (based on HY 130). Experimenting on a specimen of yield stress $\sigma_0 = 1060\,\text{MPa}$, they observed hydrogen induced cracking along shear bands at the notch root and they termed it plasticity related hydrogen induced cracking (PRHIC). It is notable that this PRHIC was observed at high strains prior to specimen failure and in the absence of sufficient impurity segregation. In this case the results of the present study suggest that the preponderance of the hydrogen resides at the notch root when the plasticity is fully developed across the unnotched ligament. On the other hand, a notched specimen of a heat aged 1000h (to allow segregation of embrittling elements like Mn and Si, to grain boundaries), $\sigma_0 = 1015\,\text{MPa}$, microcracked intergranularly at a load less than half of the general yield load in the region between the notch tip and the hydrostatic stress peak location. According to the present study calculations for high strength steels the hydrogen building-up location is inward from the notch root at the hydrostatic stress location when the plasticity is limited. Takeda and McMahon maintain that this intergranular hydrogen induced cracking (IGHIC) tends to be the dominant mode of embrittlement in practice, particularly in the early stages of cracking. Similar modes of PRHIC and IGHIC were also observed experimentally on four-point bend tests of Sb-doped Ni-Cr medium strength steel ($\sigma_0 = 840\,\text{MPa}$) by

Kameda and McMahon [125] and Morgan [126]. However, the present calculations do not address medium strength levels, even though a similar assessment for the site of maximum hydrogen concentration as in high strength steels may still apply.

Costa and Thompson [135] investigated the effect of hydrogen on the fracture behavior of a quenched and tempered at various temperatures medium-carbon 1045 steel. For a tempering temperature of 400C the yield stress was found to be $\sigma_0 = 1225\,\text{MPa}$ and this allows the use of the results of Figs. 22 and 23 in interpreting the hydrogen distribution ahead of the rounded notch in the slow bend tests they conducted on a specimen similar to that of Griffiths and Owen [118]. For this steel crack initiation in the uncharged specimen took place at a load such that $\sigma_{nom}/\sigma_0 = 2.88$, and $\sigma_{nom}/\sigma_0 = 0.66$ in the presence of hydrogen. At this low level of nominal load, it can be inferred from Figs. 22, 23 that hydrogen should have accumulated at the hydrostatic stress peak location at a distance $R \approx 0.75 r_0$ from the notch root. Costa and Thompson report that the crack initiation event was infrequently identified, because in most cases some propagation of the crack occurred before the loading could be stopped. Thus it is likely that sub-surface crack initiation might have occurred accompanied by almost simultaneous brittle intergranular fracture with sections of transgranular quasi-cleavage of the uncracked ligament.

Later results by Costa and Thompson [136] in nominally pearlitic 1045 steel ($\sigma_0 = 590\,\text{MPa}$) cannot be addressed with the present study because the yield stress of the material is neither low (low strength) nor very large (high strength). However, since fracture initiation was observed to occur just prior to general yielding of the specimen, trapping of hydrogen should have dominated the hydrogen distribution whose maximum should have developed close to the notch root. The authors had difficulties in determining the cracking location but they claim that the location of crack initiation shifted from notch root surface to subsurface with the addition of

hydrogen.

In summary, the finite element calculations of the hydrogen accumulation site ahead of a rounded notch subjected to stress are in correspondence with experimental findings on the location of the crack initiation site. When fracture is accompanied by large strains at the notch root, most of the hydrogen is trapped close to the notch root and cracking has been observed to initiate there. In contrast, when limited plastic straining precedes the fracture event most of the hydrogen resides at the NILS sites at the hydrostatic stress peak location inside from the tip. At these occasions hydrogen has been reported to induce microcracking in the highly stressed material volume inside from the notch root.

8. CONCLUSIONS

The coupled hydrogen diffusion initial boundary value problem and the large strain elastic-plastic boundary value problem was solved in the neighborhood of a blunting crack tip at a pre-cracked specimen and of a rounded notch at a 4-point bend specimen. The calculations were carried out at room temperature under plane strain conditions using material parameters for steel (low hydrogen solubility) and niobium systems (high hydrogen solubility). Both zero flux and constant hydrogen concentration boundary conditions were used. The numerical results can be summarized as follows [52]:

i) Since the Oriani's equilibrium theory between the trap and NILS populations was used trapped hydrogen concentrations become larger than the NILS concentrations with increasing plastic strain and decreasing initial concentration.

ii) In pre-cracked steel specimens strained under small scale yielding conditions, hydrogen trapping dominates the hydrogen populations regardless of the strength level of steel. As a result, hydrogen accumulates at the surface at the crack tip and not at the hydrostatic stress peak location further inside from the tip.

iii) In pre-cracked niobium specimens strained under small scale yielding, trapping concentrations dominate at small initial concentrations (i.e., less than or equal to 10^{-4}hydrogen atoms per metal atom) and the accumulation site is the crack tip free surface. However, at large initial concentrations (i.e., greater than or equal to 10^{-2}) the NILS concentrations dominate resulting in hydrogen concentration profiles ahead of the tip with the local maximum being at the hydrostatic stress peak location.

iv) In 4-point bend specimens of low strength steels $\sigma_0 \leq 250\text{MPa}$, NILS populations dominate if the plastic strains at the notch are small (less than 0.5% at $\sigma_{nom}/\sigma_0 \sim 1.0$). At larger strains, trapping populations dominate as in the case of pre-cracked specimens under small scale yielding conditions. In high strength steels, NILS dominance holds at even higher plastic strains at the notch root (~2.3%, $\sigma_{nom}/\sigma_0 \sim 1.0$). In general, for both low and high strength steels trapped populations dominate when the load is raised to values close and beyond the general yield load.

v) In experimental studies with 4-point bend specimens hydrogen induced cracking at the surface of the notch occurred under large strains and microcracking inside from the notch was the case at very small strains. These results, in conjunction with the present numerical calculations of the hydrogen concentration point to the direction that most of the hydrogen was residing at the microcrack initiation site prior to the onset of fracture.

vi) The present hydrogen transport model results, although very helpful in understanding the interaction of hydrogen with local elastoplasticity, do not reveal the role of hydrogen in promoting material degradation. Further research is needed in the direction of coupling the present model results with the actual embrittling mechanism(s) (HELP or decohesion) operating in the microscale. For instance, incorporation of the shielding mechanism for embrittlement [25] in the present

calculations may help to elucidate the role of hydrogen in promoting shear localization of the plastic flow under certain temperature and strain rate conditions.

ACKNOWLEDGEMENTS

This work was supported by the Department of Energy under grant DEFGO2-91ER45439.

REFERENCES

1. Birnbaum, H. K. and Sofronis, P., Hydrogen-enhanced localized plasticity-a mechanism for hydrogen related fracture. *Mater. Sci. &* Engng, 1994, **A176**, 191-202.
2. Birnbaum, H. K., Hydrogen related failure mechanisms in metals. In *Environmental Sensitive Fracture of Engineering Materials* (Proceedings of Symposium on Environmental Effects on Fracture, Chicago, Illinois, October 24-26, 1977), ed. Z. A. Foroulis, Metallurgical Society of AIME, Warendale, PA, 1979, pp. 326-360.
3. Birnbaum, H. K., Hydrogen related fracture of metals. In *Atomistics of Fracture* (Proceedings of a NATO Advanced Research Institute on Atomistics of Fracture, Calcatoggio, Corsica, France, May 22-31, 1981), ed. R. A. Latanision and J. R. Pickens, Plenum Press, New York, 1983, pp. 733-765.
4. Birnbaum, H. K., Hydrogen related second phase embrittlement of solids. In *Hydrogen Embrittlement and Stress Corrosion Cracking*, (Proceedings of a Troiano Festschrift Symposium, Case Western Reserve University, June 1-3, 1980), ed. R. Gibala and R. F. Hehemann, ASM Ohio, 1984, pp. 153-177.
5. Hirth, J. P., Theories of hydrogen induced cracking of steels. In *Hydrogen Embrittlement and Stress Corrosion Cracking*, (Proceedings of a Troiano Festschrift Symposium, Case Western Reserve University, June 1-3, 1980), ed. R. Gibala and R. F. Hehemann, ASM Ohio, 1984, pp. 29-41.
6. Johnson, H. H., Overview of hydrogen degradation phenomena. In *Hydrogen Embrittlement and Stress Corrosion Cracking*, (Proceedings of a Troiano Festschrift Symposium, Case Western Reserve University, June 1-3, 1980), ed. R. Gibala and R. F. Hehemann, ASM Ohio, 1984, pp. 3-27.
7. Hirth, J. P., Effects of hydrogen on the properties of iron and steel. *Met Trans.*, 1980, **11A**, 861-890.
8. Birnbaum, H. K., Robertson, I. M., Sofronis P. and Teter, D., Mechanisms of hydrogen related fracture—A review. In *Corrosion Deformation Interactions CDI'96* , (Second International Conference, Nice, France, 1996), ed. T. Magnin,

The Institute of Materials, Great Britain, 1997, pp. 172-195.

9. Birnbaum, H. K., Environment-induced cracking of metals. In *Environment-induced cracking of metals* (First International Conference, Kohler, Wisconsin, 1988), ed. R. P. Gangloff and M. B. Ive, NACE, Houston, TX, 1988, pp. 21-29.

10. Price, E. G., Highlights of the metallurgical behaviour of CANDU pressure tubes. AECL technical report, Chalk River, Ontario, Canada, 1984.

11. Teter, D. F., The Effects of hydrogen on the deformation and fracture behavior of the metastable beta-titanium alloy, timetal 21S. PhD dissertation, University of Illinois at Urbana-Champaign, Urbana, Illinois, 1996.

12. Westlake, D. G., A generalized model for hydrogen embrittlement. *Trans. ASM*, 1969, **62**, 1000-1006.

13. Birnbaum, H. K., Grossbeck M. L. and Amano M., Hydride precipitation in Nb and some properties of NbH. *J. Less Comm. Met.*, 1976, **49**, 357-370.

14 Gahr, S., Grossbeck, M. L. and Birnbaum, H. K., Hydrogen embrittlement of Nb I - Macroscopic behavior at low temperatures. *Acta Metall.*, 1977, **25**, 125-134.

15. Grossbeck, M. L. and Birnbaum, H. K., Low temperature hydrogen embrittlement of niobium II - Microscopic observations. *Acta Metall.*, 1977, **25**, 135-147.

16 Shih, D., Robertson, I. M. and Birnbaum, H. K., Hydrogen embrittlement of α titanium: in situ TEM studies. *Acta Metall.*, 1988, **36**, 111-124.

17 Lufrano, J., Sofronis, P. and Birnbaum, H. K., Modeling of hydrogen transport and elastically accommodated hydride formation near a crack tip. *J. Mech. Phys. Solids*, 1996, **44**, 179-205.

18 Lufrano, J., Sofronis, P. and Birnbaum, H. K., Elastoplastically accommodated hydride formation and embrittlement. *J. Mech. Phys. Solids*, 1998, **46**, 1497-1520.

19. Beachem, C. D., A new model for hydrogen-assisted cracking (hydrogen embrittlement). *Met. Trans.*, 1972, **3**, 437-451.

20. Meyers, S. M. *et al.*, Hydrogen interactions with defects in crystalline solids. *Rev. Mod. Phys.*, 1992, **64**, 559-617.

21. Sirois, E., Sofronis, P. and Birnbaum, H. K., Effects of hydrogen and carbon on thermally activated deformation in nickel. In *Parkins Symposium on Fundamental Aspects of Stress Corrosion Cracking* , ed. S. M. Bruemmer, E. I. Meletis, R. H. Jones, W. W. Gerberich, F. P. Ford, and R. W. Staehle, The Minerals, Metals & Materials Society, 1992, pp. 173-190.

22. Sirois, E. and Birnbaum, H. K., Effects of hydrogen and carbon on thermally activated deformation in nickel. *Acta Metall.*, 1992, **40**, 1377-1385.

23. Birnbaum, H. K., Mechanisms of hydrogen related fracture of metals. In *Hydrogen Effect on Materials Behavior*, ed. N. Moody and A. W. Thompson,

The Minerals, Metals and Materials Society, New York, 1990, pp. 639-658.

24. Birnbaum, H. K., Hydrogen effects on deformation-relation between dislocation behavior and the macroscopic stress-strain behavior. *Scr. met.*, 1994, **31** 149-153.

25. Sofronis, P. and Birnbaum, H. K. Mechanics of the hydrogen-dislocation-impurity interaction—I. Increasing shear modulus. *J. Mech. Phys. Solids*, 1995, **43**, 49-90.

26. Troiano, A. R., The role of hydrogen and other interstitials in the mechanical behavior of metals. *Trans. ASM*, 1960, **52**, 54-80.

27. H. H. Johnson, H. H., J. G. Morlet, J. G. and Troiano, A. R., Hydrogen, crack initiation, and delayed failure in steel. *Trans. Met. Soc. AIME*, 1958, **212**, 528-536.

28. Steigerwald, E. A., Schaller, F. W. and Troiano, A. R., The role of stress in hydrogen induced delayed failure. *Trans. Met. Soc. AIME*, 1960, **218**, 832-841.

29. Oriani, R. A. and Josephic, P. H., Equilibrium aspects of hydrogen-induced cracking of steels. *Acta Metall.*, 1974, **22**, 1065-1074.

30. Oriani, R. A. and Josephic, P. H., Equilibrium and kinetic studies of the hydrogen-assisted cracking of steel. *Acta Metall.*, 1977, **25**, 979-988.

31. Gerberich, W. W. and Chen, Y. T., Hydrogen-controlled cracking – An approach to threshold stress intensity. *Metall. Trans.*, 1975, **6A**, 271-278.

32. Lessar, J. F. and Gerberich, W. W., Grain size effects in hydrogen-assisted cracking *Metall. Trans.*, 1976, **7A**, 953-960.

33. Gahr, S. and Birnbaum, H. K., Hydrogen embrittlement of niobium—III. High temperature behavior. *Acta Metall.*, 1978, **26**, 1781-1788.

34. Sherman, D. H., Owen, C. V. and Scott, T. E., The effect of hydrogen on structure and properties of vanadium. *Trans. AIME*, 1968, **242**, 1775-1784.

35. Hardie, D. and McIntyre, P., The low-temperature embrittlement of niobium and vanadium by both dissolved and precipitated hydrogen. *Metall. Trans.*, 1973, **4**, 1247-1254..

36. Paton, N. E. and Williams, J. C., Effect of hydrogen on titanium and its alloys. In *Hydrogen in Metals*, ed. I. M. Bernstein and A. W. Thompson, ASM, Metals Park, Ohio, 1973, pp. 409-431.

37. Dutton, R., Nuttall, K., Puls, M. P. and L. A. Simpson, Mechanisms of hydrogen induced delayed cracking in hydride forming materials. *Met. Trans.*, 1977, **8A**, 1553-1562.

38. Takano, S. and Suzuki, T., An electron optical study of b-hydride and hydrogen embrittlement of vanadium. *Acta Metall.*, 1974, **22**, 265-274.

39. Flannagan, T. B., Mason, N. B. and Birnbaum, H. K., The effect of stress on hydride precipitation. *Scripta Met.*, 1981, **14**, 109-112.

40. Tabata, T. and Birnbaum, H. K., Direct observations of the effect of hydrogen on

the behavior of dislocations in iron. *Scripta Met.*, 1983, **17**, 947-950.

41. Tabata, T. and Birnbaum, H. K., Direct observations of hydrogen enhanced crack propagation in iron. *Scripta Met.*, 1984, **18** , 231-236.

42. Robertson, I. M. and Birnbaum, H. K., An HVEM study of hydrogen effects on the deformation and fracture of nickel. *Acta Metall.*, 1986, **34**, 353-366.

43. Bond, G. M., Robertson, I. M. and Birnbaum, H. K., The influence of hydrogen on deformation and fracture processes in high-strength aluminum alloys. *Acta Metall.*, 1987, **35**, 2289-2296.

44. Bond, G. M., Robertson, I. M. and Birnbaum, H. K., Effects of hydrogen on deformation and fracture processes in high-purity aluminum. *Acta Metall.*, 1988, **36**, 2193-2197.

45. Rozenak, P., Robertson, I. M. and Birnbaum, H. K. (1990) HEVM studies of the effects of hydrogen on the deformation and fracture of AISI type 316 austenitic stainless steel. *Acta Metall.*, 1990, **38**, 2031-2040.

46. Eastman, J., Matsumoto, T., Narita, N., Heubaum, N. and Birnbaum, H. K., Hydrogen effects in nickel embrittlement or enhanced ductility? In *Hydrogen in Metals*, ed. I. M. Bernstein and A. W. Thompson, Metallurgical Society of AIME, New York, 1981, pp. 397-409.

47. Daw, M. S and Baskes, M. I., Embedded-atom method: derivation and application to impurities, surfaces, and other defects in metals. *Phys. Rev.*, 1984, **29B**, 6443-6453.

48. Hirth, J. P. and Rice, J. R., On the thermodynamics of adsorption at interfaces as it influences decohesion. *Metall. Trans.*, 1980, **11A**, 1501-1511.

49. Hirth, J. P., Interfacial decohesion. *Phil. Trans. Royal Soc. Lon.*, 1980, **295A**, 139-149.

50. J. R. Rice Mechanics aspects of stress corrosion cracking and hydrogen embritllement, In *Stress Corrosion Cracking and Hydrogen embrittlement of Iron Base Alloys*, ed. R. W. Staehle, J. Hochmann, R. D. McCright and J. E. Slater, NACE, TX, 1977, NACE-5, pp. 11-15.

51. Rice, J. R., Some mechanics research topics related to the hydrogen embrittlement of metals. *Corrosion*, 1976, **32**, 22-26.

52. Lufrano, J and Sofronis, P., Enhanced hydrogen concentrations ahead of rounded notches and cracks—competition between plastic strain and hydrostatic stress. *Acta mater.*, 1998, **46**, 1519-1526.

53. Lufrano, J., Symons, D. and Sofronis, P., Hydrogen transport and large strain elastoplasticity near a notch in alloy X-750. *Eng. Fract. Mech.*, 1998, **59**, 827-845.

54. Cottrell, H. A., Effects of solute atoms on the behavior of dislocations. In *Report of a conference on Strength of Solids*, The Physical Society, London, 1948, pp. 30-36.

55. Eshelby, J. D., The elastic interaction of point defects. *Acta Metall.*, 1955, **3**, 487-490.

56. Eshelby, J. D., The continuum theory of lattice defects. In *Solid State Physics*, ed. F. Seitz and D. Turnbull, Academic Press, New York, 1956, **3**, 79-144.

57. Eshelby, J. D., The determination of the elastic field of an ellipsoidal inclusion and related problems. *Proc. R. Soc. London*, 1957, **241A**, 376-396.

58. Hirth, J. P. and Lothe, J., Theory of Dislocations, John Wiley & Sons Inc., New York, 1982, pp. 487-530.

59. Peisl, H. Lattice strains due to hydrogen in metals. In *Hydrogen in Metals I, Topics in Applied Physics*, ed. G. Alefeld and J. Volkl, Springer, New York, 1978, **28**, 53-74, .

60. Mazzolai, F. M. and Birnbaum, H. K., Elastic constants and ultrasonic attenuation of the 'alpha—alpha' phase of the Nb-H(D) system. I. Results. *J. Phys. F: Met. Phys.*, 1985, **15**, 507-523,

61. F. M. Mazzolai and H. K. Birnbaum, Elastic constants and ultrasonic attenuation of the 'alpha—alpha' phase of the Nb-H(D) system. II. Interpretation of results. *J. Phys. F: Met. Phys.*, 1985, **15**, 525-542.

62. Li, J. C. M., Oriani, R. A. and Darken, L. S. The thermodynamics of stressed solids. *Z. Physik Chem. Neue Folge*, 1966, **49**, 271-291.

63. Larche, F. C. and Cahn, J. W., The interaction of composition and stress in crystalline solids. *Acta Metall.*, 1985, **33**, 331-357.

64. Sofronis, P., The influence of mobility of dissolved hydrogen on the elastic response of a metal. *J. Mech. Phys. Solids*, 1995, **43**, 1385-1407.

65. Tien, J. K., Nair, S. V. and Jensen R. R., Dislocation sweeping of hydrogen and hydrogen embrittlement. In *Hydrogen Effects in Metals* ed. I. M. Bernstein and A. W. Thompson, *Metallurgical Society of AIME*, New York, NY, 1981, pp. 37-56.

66. Frankel, G. S. and Latanision, R. M., Hydrogen transport during deformation in nickel: Part I polycrystalline nickel. *Met. Trans.*, 1986, **17A**, 861-867.

67. Ladna, B. and Birnbaum, H. K., A study of hydrogen transport during plastic deformation. *Acta Metall.*, 1987, **35**, 1775-1778.

68. Wert, C. A., Trapping of hydrogen in metals. In *Hydrogen in Metals I, Topics in Applied Physics*, ed. G. Alefeld and J. Volkl, Springer-Verlag, New York, 1978, Vol. 29, pp. 305-330.

69. Wert, C. A. and Frank, R. C., Trapping of interstitials in metals. *Ann. Rev. Mater. Sci.*, 1983, **13**, 139-172.

70. R. Gibala, R. and Kumnick, A. J., Hydrogen trapping in iron and steels. In *Proceedings of a Troiano Festschrift Symposium*, held at Case Western Reserve University, June-1-3, 1980. ed. R. Gibala and R. F. Hehemann, ASM, Ohio, 1984,

Vol. **29**, pp. 61-77.

71. Bernstein, I. M., Garber, R. and Pressouyre, G. M., Effect of dissolved hydrogen on mechanical behavior of metals. In *Effect of Hydrogen on Behavior of Materials*, ed. A. W. Thompson and I. M. Bernstein, Metallurgical Society of AIME, New York, 1976, pp. 37-57.

72. Gibala, R., Hydrogen—defect interactions in iron—base alloys. In *Stress Corrosion Cracking and Hydrogen embrittlement of Iron Base Alloys*, ed. R. W. Staehle, J. Hochmann, R. D. McCright and J. E. Slater, NACE, TX, 1977, NACE-5, pp. 244-271.

73. Pressouyre, G. M., Trap theory of hydrogen embrittlement. *Acta Metall.*, 1980, **28**, 895-911.

74. Bernstein, I. M. and Pressouyre, G. M., The role of traps in the microstructural control of hydrogen embrittlement of steels. In *Hydrogen Degradation of Ferrous alloys*, ed. R. A. Oriani, J. P. Hirth and M. Smialowski, Noyes Publications, New Jersey, 1985, pp. 641-685.

75. Pressouyre, G. M., and Bernstein, I. M., A quantitative analysis of hydrogen trapping. *Metall. Trans.*, 1978, **9A**, 1571-1580.

76. Pressouyre, G. M., and Bernstein, I. M., An example of the effect of hydrogen trapping on hydrogen embrittlement. *Metall. Trans.*, 1981, **12A**, 835-844.

77. Thompson, A. W. and Bernstein, I. M., The role of metallurgical variables in hydrogen-assisted environmental fracture. In *Advances in Corrosion Science and Technology*, ed. M. G. Fontana and R. W. Staehle, Plenum Press, New York, 1980, Vol. **7**, pp. 83-175.

78. Tuyen, D. L. and Bernstein, I. M., Hydrogen trapping of spheroidized steels as a function of plastic strain. *Scr. Met.*, 1986, **20**, 1025-1029.

79. Kumnick, A. J., and Johnson, H. H., Hydrogen transport through annealed and deformed iron. *Metall. Trans*, 1974, **5A**, 1199-1206.

80. Oriani, R. A., The diffusion and trapping of hydrogen in steel. *Acta Metall.*, 1970, **18**, 147-157.

81. Kumnick, A. J., and Johnson, H. H., Deep trapping states for hydrogen in deformed iron. *Acta Metall.*, 1980, **28**, 33-39.

82. Johnson, H. H. and R. W. Lin, R. W., Hydrogen and deuterium trapping in iron. In *Hydrogen Effects in Metals*, ed. I. M. Bernstein and A. W. Thompson, Metallurgical Society of AIME, New York, 1981, pp. 3-23.

83. Thomas, G. J. Hydrogen trapping in FCC metals. In *Hydrogen Effects in Metals*, ed. A. W. Thompson and I. M. Bernstein, *Trans. Met. Soc. AIME*, New York, NY, 1980, pp. 77-85.

84. Angelo, J. E., Moody, N. R. and Baskes, M. I., Modeling the segregation of hydrogen to lattice defects in nickel. In *Hydrogen Effects in Materials*, eds. A. W. Thompson and N. R. Moody, *Trans. Met. Soc. AIME*, New York, NY, 1996,

pp. 161-170.

85. Tien, J. K., Thompson, A. W., Bernstein, I. M., and Richards, R. J. Hydrogen transport by dislocations. *Metall. Trans.*, 1976, **7A**, 821–829.

86. McLellan, R. B., Thermodynamics of diffusion behavior of interstitial solute atoms in non-perfect solvent crystals. *Acta Metall.*, 1979, **27**, 1655-1663.

87. Symons, D. M. An investigation into the effects of hydrogen on the fracture and deformation behavior of alloy-X-750. Ph.D. dissertation, Carnegie Mellon University, Pittsburgh, PA, 1994.

88. Turnbull, A., Ballinger, R. G., Hwang, Morra, M. M., Psaila-Dombrowski, M. and Gates, R. M., Hydrogen transport in nickel-base alloys. *Met. Trans.*, 1992, **23A**, 3231-3244.

89. Van Leeuwen, H. P., The kinetics of hydrogen embrittlement: a quantitative diffusion model. *Eng. Fract. Mech.*, 1974, **6**, 141-161.

90. Hippsley, C. A. and Briant, C. L., Application of a model for stress driven segregation to hydrogen embrittlement. *Scr. Met.*, 1985, **19**, 1203-1208.

91. Liu, H. W., Stress-corrosion cracking and the interaction between crack-tip stress field and solute atoms, *J. Basic Engng* Trans. ASME, 1970, **92**, 633-638.

92. Tong-Yi, Z., Mason, T. A. and Hack, J. E., The equilibrium concentration of hydrogen atoms ahead of mode I crack tip single crystal iron. *Scr. Met.*, 1992, **26**, 139-144.

93. Tong-Yi, Z., Shen, H. and Hack, J. E., The influence of cohesive forces on the equilibrium concentration of hydrogen atoms ahead of a crack tip in single crystal iron. *Scr. Met.*, 1992, **27**, 1605-1610.

94. Unger, D. J., A mathematical analysis for impending hydrogen assisted crack propagation. *Eng. Fracture Mech.*, 1989, **34**, 657-667.

95. Lufrano, J. and Sofronis, P., Numerical analysis of the interaction of solute hydrogen atoms with the stress field of a crack. *Int. J. Solids Structures*, 1996, **33**, 1709-1723.

96. McNabb and P. K. Foster, A new analysis of the diffusion of hydrogen in iron and ferritic steels. *Trans. Met. Soc. AIME*, 1963, **227**, 618-627.

97. Pressouyre, G. M., A classification of hydrogen traps in steel. *Metall. Trans*, 1979, **10A**, 1571-1573.

98. Pressouyre, G. M., and Bernstein, I. M., A kinetic trapping model for hydrogen-induced cracking. *Acta Metall.*, 1979, **27**, 89-100.

99. Foster, P. K., McNabb, A. and Payne, C. M., On the rate of loss of hydrogen from cylinders of iron and steel. *Trans. Met. Soc. AIME*, 1965, **233**, 1022-1031.

100. Booth, D. M. A., and Hewitt, J., A mathematical model describing the effects of microvoids upon the diffusion of hydrogen in iron and steel. *Acta Metall.*, 1974, **22**, 171-175.

101. Booth, D. M. A., Atkinson, C. and Bilby B. A., A numerical solution of the diffusion equation resulting from the void theory of the trapping of hydrogen in iron and steel. *Acta Metall.*, 1975, **23**, 371-376.

102. Caskey, G. R. and Pillinger, W. L., Effect of trapping on hydrogen permeation. *Metall. Trans.*, 1975, **6A**, 467-476.

103. Frank, R. C., Wert, C. W. and Birnbaum, H. K., Modeling diffusion through non-uniform concentrations of traps. *Metall. Trans.*, 1979, **10A**, 1627-1630.

104. Thomas, P. G. and Stern, E. J., Efficient numerical modeling of hydrogen diffusion with trapping. *J. Mater. Sci.*, 1981, **16**, 3122-3130.

105. Ellebrock, Von H. G., Vibrans, G. and Stuwe, H. P., Diffusion von wasserstoff in stahl mit inneren hohlraumen. *Acta Metall.*, 1972, **20**, 53-60.

106. Allen-Booth, D. M., Atkinson, C. and Bilby, B. A., A numerical solution of the diffusion equation resulting from the void theory of the trapping of hydrogen in iron and steel. *Acta Metall.*, 1975, **23**, 371-376.

107. Kitagawa, H. and Kojima, Y. Diffusion of hydrogen near an elasto-plastically deformed crack tip. In*Atomistics of Fracture* (Proceedings of a NATO Advanced Research Institute on Atomistics of Fracture, Calcatoggio, Corsica, France, May 22-31, 1981), ed. R. A. Latanision and J. R. Pickens, Plenum Press, New York, 1983, pp. 799-811.

108. Sofronis, P. and McMeeking, R. M., Numerical analysis of hydrogen transport near a blunting crack tip. *J. Mech. Phys. Solids*, 1989, **37**, 317-350.

109. Krom, A. H. M., Numerical modeling of hydrogen transport in steel. Ph.D. dissertation, Delft University Press, Delft, The Netherlands, 1998.

110. Sun, S., Shiozawa, K., Gu, J., and Chen, N., Investigation of deformation field and hydrogen partition around crack tip in fcc single crystal. *Metallurgical and Materials Transactions*, 1995, **17**, 1213-1220.

111. McMeeking, R. M. and Rice, J. R., Finite-element formulations for problems of large elastic-plastic deformation. *Int. J. Solids Structures*, 1975, **11**, 601-616.

112. Govindarajan, R. M. and Aravas, N., Deformation processing of metal powders: Part I—Cold isostatic pressing. *Int. J. Mech. Sci.*, 1994, **36**, 343–357.

113. Nagtegaal, J. C., Parks, D. M. and Rice, J. R., On numerically accurate finite element solutions in the fully plastic range. *Comp. Meth. Appl. Mech. Eng.*, 1974, **4**, 153-177.

114. Irwin, G. R., Fracture Mechanics. In *Structural Mechanics* (Proceedings of the First Symposium of Naval Structural Mechanics), ed. J. N. Goodier and N. J. Hoff, Stanford University, 1960, pp. 557-594.

115. Völkl, J. and Alefeld, G., Diffusion of hydrogen in metals. In *Hydrogen in Metals I, Topics in Applied Physics*, ed. G. Alefeld and J. Volkl, Springer-Verlag, New York, 1978, Vol. **28**, pp. 53-74.

116. Baker, C. and Birnbaum, H. K., On the hydrogen-dislocation interaction in niobium. *Scr. Met.*, 1972, **6**, 851-854.

117. Gilman, J. J., *Micromechanics of flow in solids*, McGraw-Hill book Company, New York, 1969, pp. 185-199.

118. Griffiths, J. R. and Owen, D. R. J., An elastic-plastic stress analysis for a notched bar in plane strain bending. *J. Mech. Phys. Solids*, 1971, **19**, 419-431.

119. Thompson, A. W. and Bernstein, I. M., Microstructure and hydrogen embrittlement. In *Hydrogen Effects in Metals*, ed. I. M Bernstein and A. W. Thompson, The Metallurgical Society of AIME, New York, 1981, pp. 291-308.

120. Lee, T. D., Goldenberg, T. and Hirth, J. P., Effect of hydrogen on fracture of U-notched bend specimens of spheroidized AISI 1095 steel. *Metall. Trans.*, 1979, **10A**, 199-208.

121. Lee, T. D., Goldenberg, T. and Hirth, J. P., Hydrogen and plastic instability in deformed speroidized 1090 steel. In *Fracture 1977*, University of Waterloo Press, Waterloo, 1977, Vol. **2**, pp. 243-248.

122. Onyewenyi, O. A. and Hirth, J. P., Effects of hydrogen on notch ductility and fracture in spheroidized AISI 1090 steel. Metall. Trans., 1983, **14A**, 259-269.

123. Lee, T. D., Goldenberg, T. and Hirth, J. P., Effect of hydrogen on fracture of U-notched bend specimens of quenched and tempered AISI 4340 steel. *Metall. Trans.*, 1979, **10A**, 439-448.

124. Takeda, Y. and McMahon, C. J. Jr., Strain controlled vs stress controlled hydrogen induced fracture in a quenched and tempered steel. *Metall. Trans.*, 1981, **12A**, 1255-1266.

125. Kameda, J. and McMahon, C. J. Jr., Solute segregation and hydrogen-induced intergranular fracture in an alloy steel. *Metall. Trans.*, 1983, **14A**, 903-911.

126. M. J. Morgan: Grain Boundary Segregation and Embrittlement by Antimony and Hydrogen in a Model Alloy Steel, PhD dissertation, University of Pennsylvania, Philadelphia, PA, 1987.

127. Yoshino, K. and McMahon, C. J. Jr., The cooperative relation between temper embrittlement and hydrogen embrittlement in a high strength steel. *Metall. Trans.*, 1974, **5**, 363-370.

128. Banerji, S. K., McMahon, C. J. Jr. and Feng, H. C., Intergranular fracture in 4340-type steels: effects of impurities and hydrogen. *Metall. Trans.*, 1978, **9A**, 237-247.

129. Briant, C. L, Feng, H. C. and McMahon, C. J. Jr., Embrittlement of a 5 pct nickel high strength steel by impurities and their effects on hydrogen-induced cracking. *Metall. Trans.*, 1978, **9A**, 625-633.

130. Bandyopadhyay, N., Kameda, J. and McMahon, C. J. Jr., Hydrogen-induced cracking in 4340-type steel: effects of composition, yield strength, and H_2 pressure. *Metall. Trans.*, 1983, **14A**, 881-888.

131. Mahon, C. J. Jr., and Vitek, V. The effects of segregated impurities on intergranular fracture energy. *Acta Metall.*, 1979, **27**, 507-513.

132. Jokl, M. L., Vitek, V. and McMahon, C. J. Jr., A microscopic theory of brittle fracture in deformable solids: a relation between ideal work of fracture and plastic work. *Acta Metall.*, 1980, **28**, 1479-1488.

133. Kameda, J. and McMahon, C. J. Jr., Solute segregation and brittle fracture in an alloy steel. *Metall. Trans.*, 1980, **11A**, 91-101.

134. Kameda, J. and McMahon, C. J. Jr., The effects of Sb, Sn, and P on the strength of grain boundaries in a Ni-Cr steel. *Metall. Trans.*, 1981, **12A**, 31-37.

135. Costa, J. E. and Thompson, A. W., Effect of hydrogen on fracture behavior of a quenched and tempered medium-carbon steel. *Metall. Trans.*, 1981, **12A**, 761-711.

136. Costa, J. E. and Thompson, A. W., Hydrogen cracking in nominally pearlitic 1045 steel. *Metall. Trans.*, 1982, **13A**, 1315-1318.

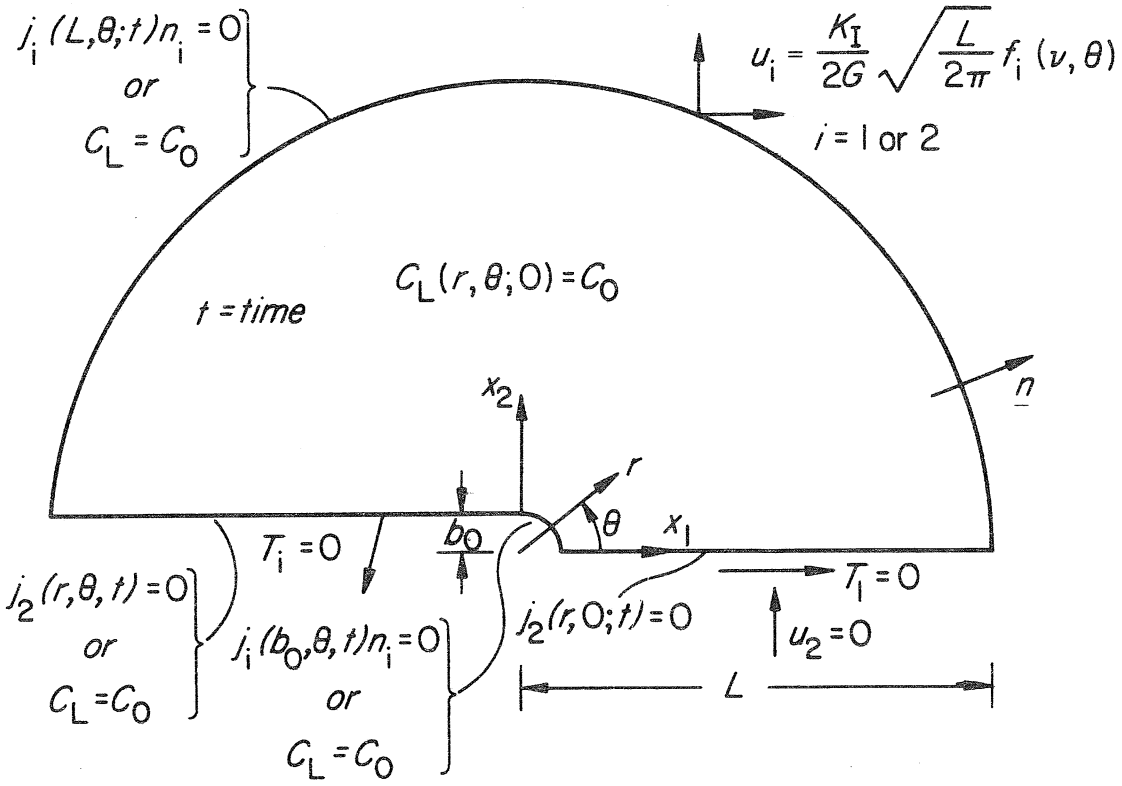

Figure 1 Description of the boundary and initial conditions for the coupled diffusion and elastic-plastic problems at a blunting crack tip under small scale yielding conditions. Constant C_0 is the initial NILS hydrogen concentration, b_0 is the crack opening displacement in the undeformed state, L is the distance from the crack tip, $\underline{n}$ is the outward unit normal to the external boundary, u_i is the displacement, K_I is the mode I applied stress intensity factor, T_i is the traction, and j_i is the hydrogen flux.

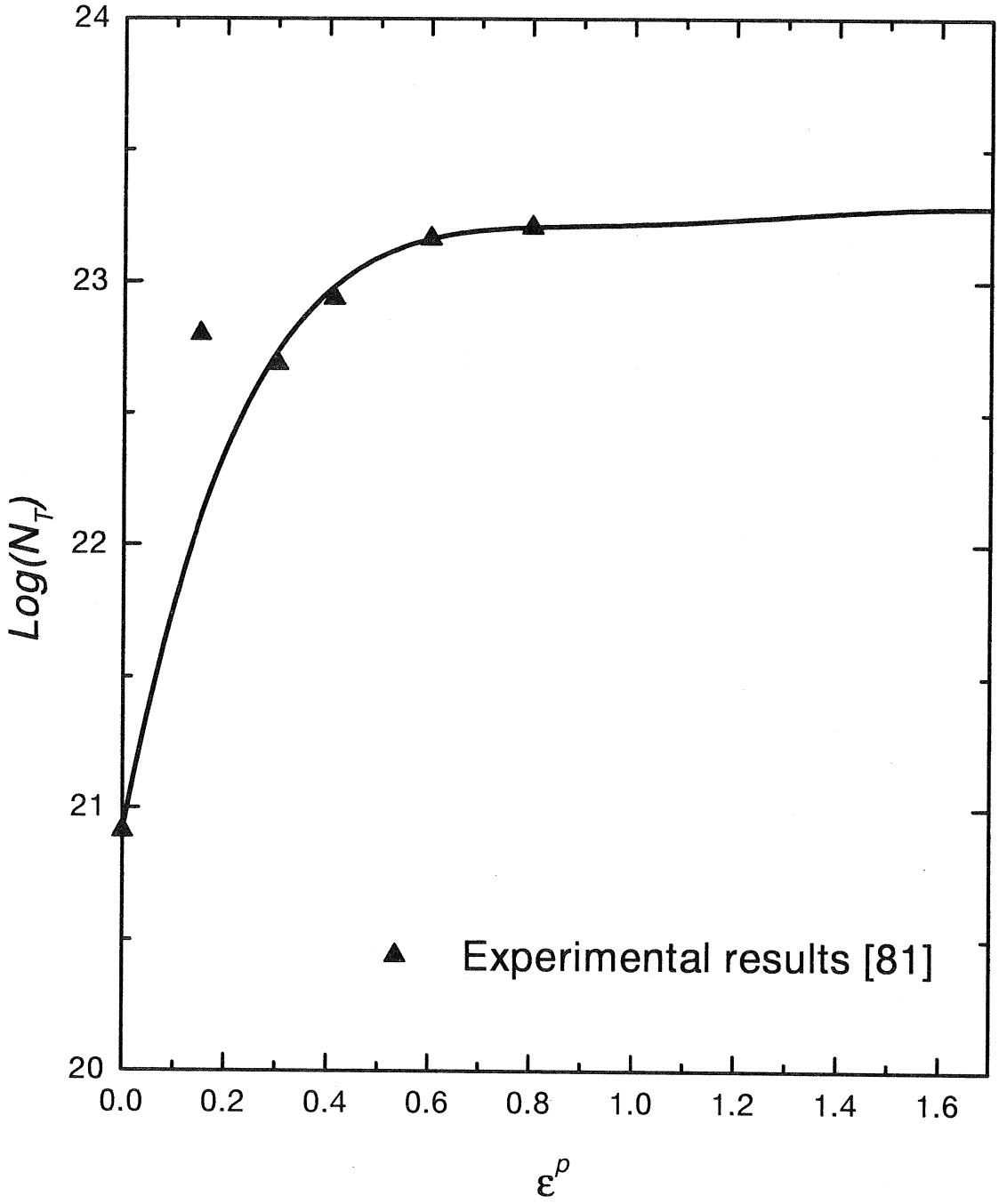

Figure 2 Relationship between the trap density N_T and the equivalent plastic strain ε^p for iron and steels [81].

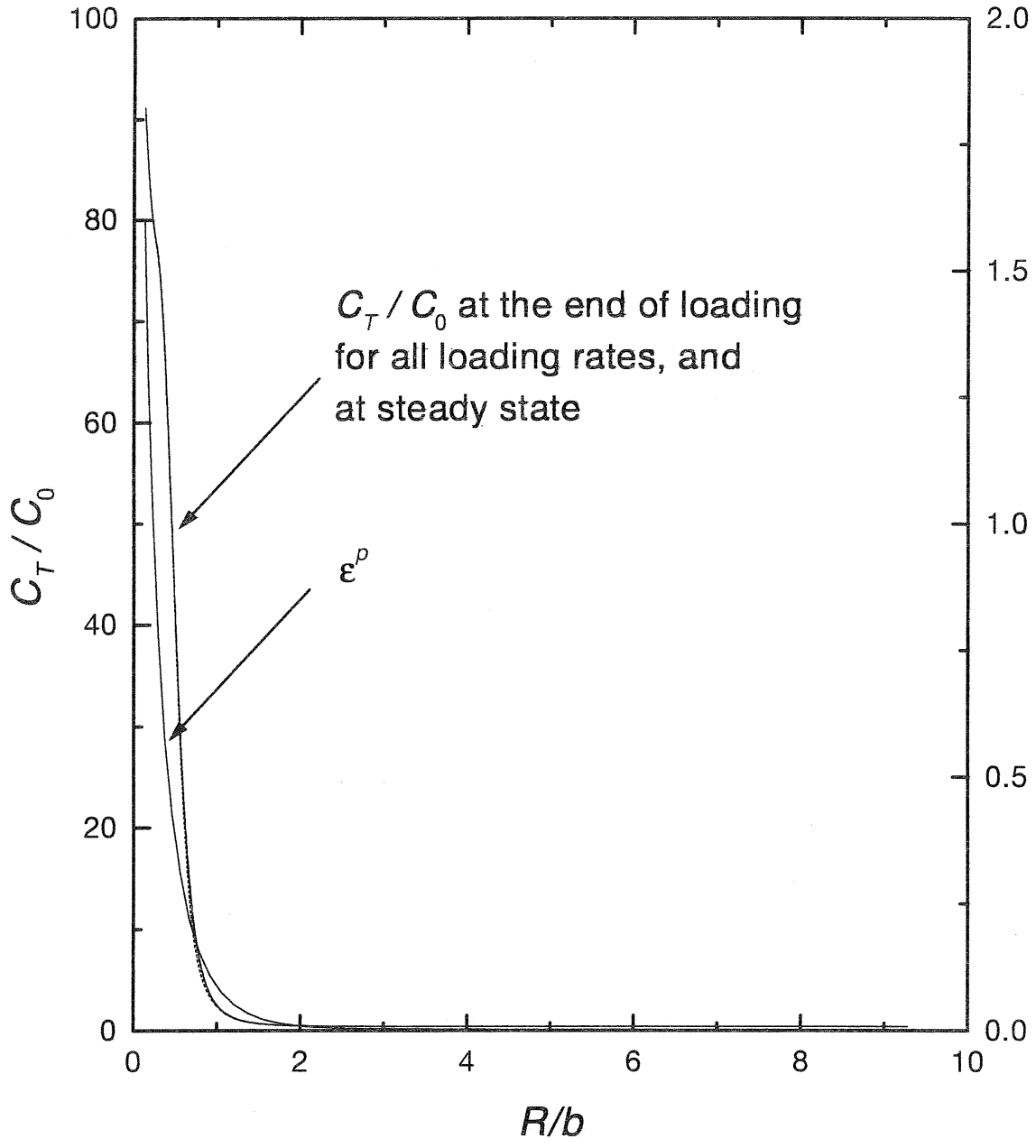

Figure 3 Plot of hydrogen concentration C_T/C_0 in trapping sites and equivalent plastic strain ε^p vs distance R/b for low strength steel ($\sigma_0 = 250\,\mathrm{MPa}$) at a blunting crack tip upon the completion of loading and at steady state under constant concentration boundary conditions. The load times were $t_l = 1.3, 13, 130\,\mathrm{s}$ and the corresponding crack opening displacement b was $5b_0$. The initial concentration C_0 equals 2.084×10^{21} hydrogen atoms per m^3.

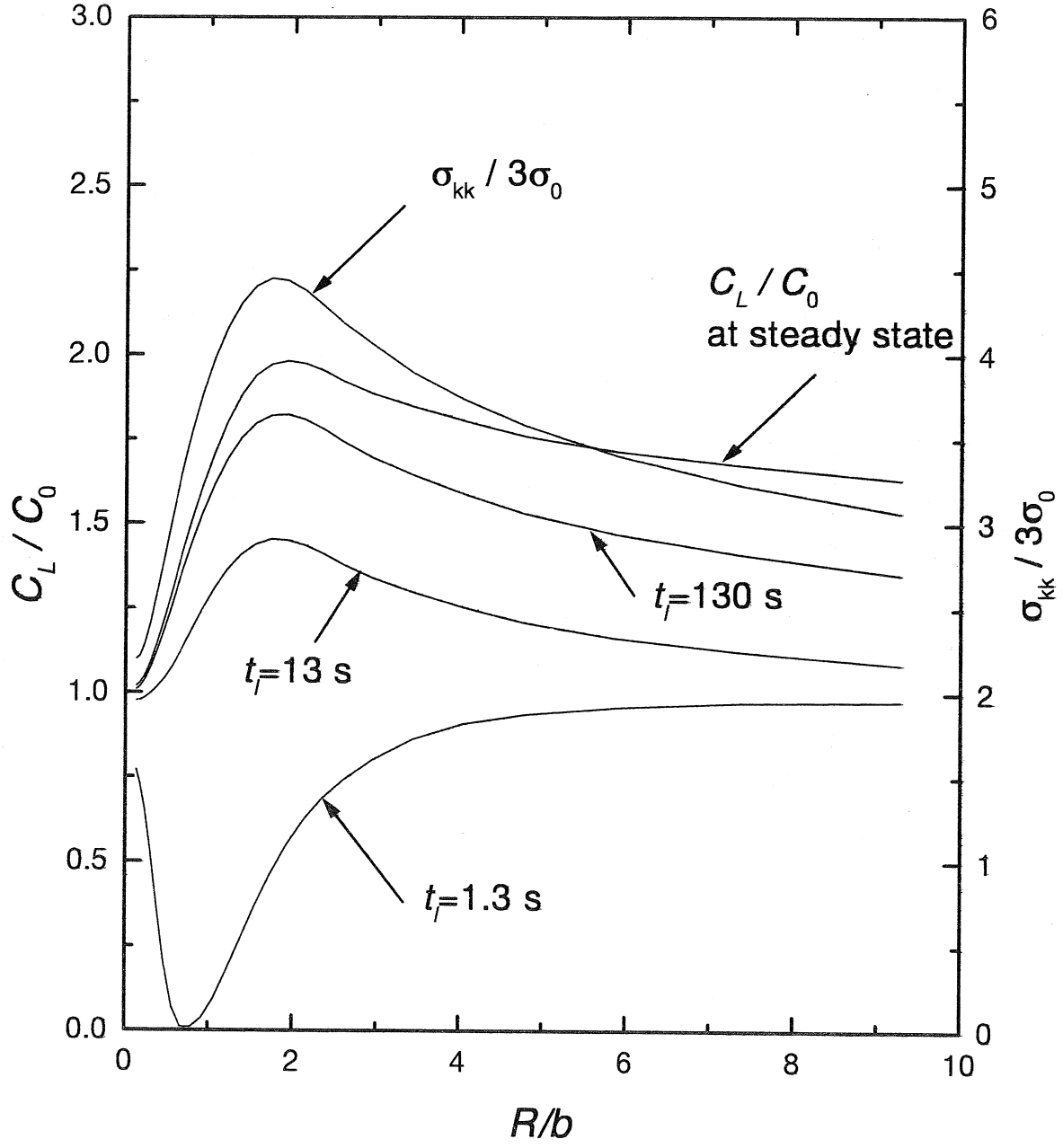

Figure 4 Plot of hydrogen concentration C_L/C_0 in NILS and hydrostatic stress $\sigma_{kk}/3\sigma_0$ vs distance R/b for low strength steel ($\sigma_0 = 250\,\mathrm{MPa}$) at a blunting crack tip upon the completion of loading and at steady state under constant concentration boundary conditions. The load times were $t_l = 1.3, 13, 130\,\mathrm{s}$ and the corresponding crack opening displacement b was $5b_0$. The initial concentration C_0 equals 2.084×10^{21} hydrogen atoms per m^3.

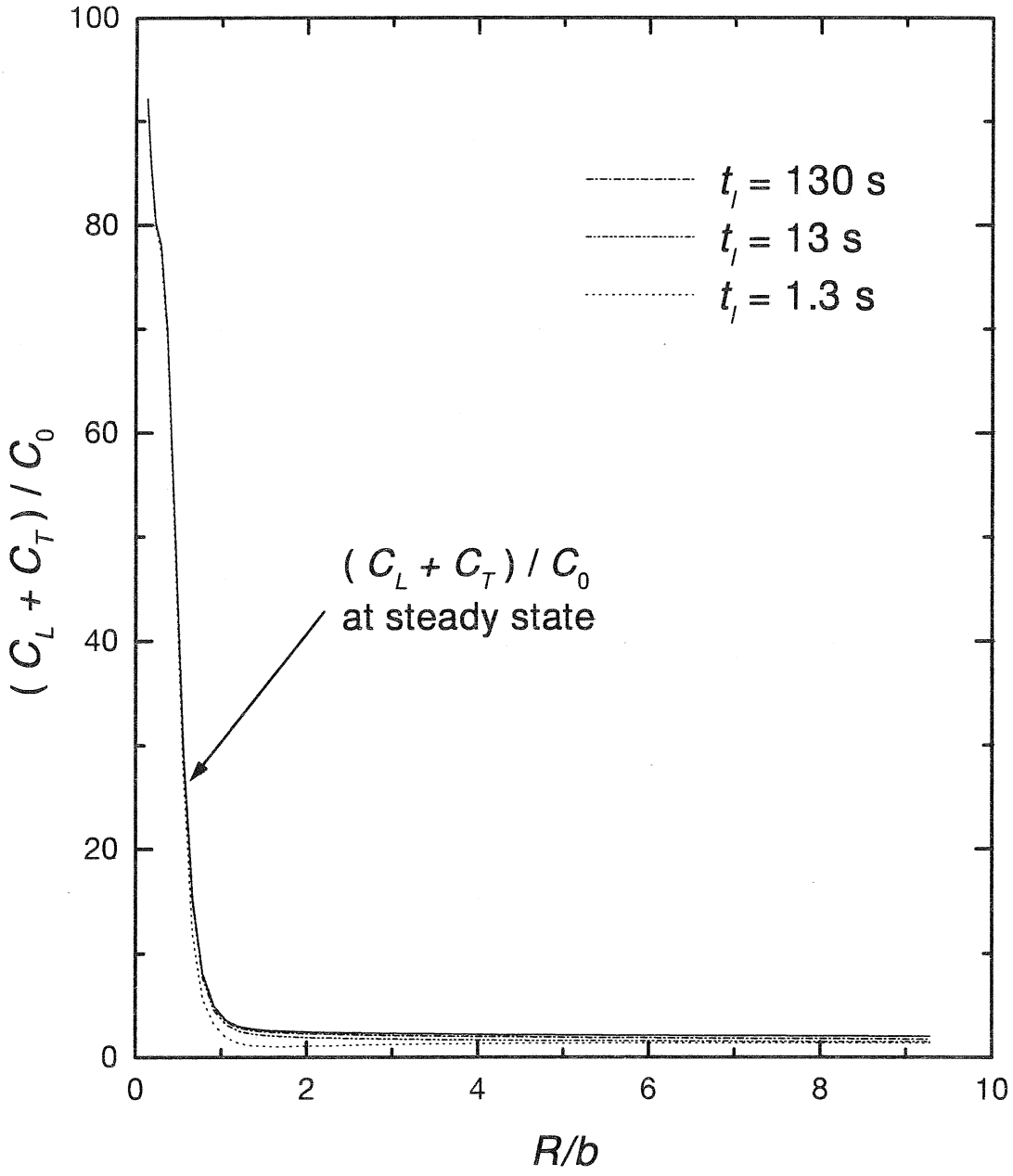

Figure 5 Plot of total hydrogen concentration $(C_L + C_T)/C_0$ **vs distance** R/b **for low strength steel** ($\sigma_0 = 250\,\mathrm{MPa}$) **at a blunting crack tip upon the completion of loading and at steady state under constant concentration boundary conditions. The load times were** $t_l = 1.3, 13, 130\,\mathrm{s}$ **and the corresponding crack opening displacement** b **was** $5b_0$. **The initial concentration** C_0 **equals** 2.084×10^{21} **hydrogen atoms per** m^3.

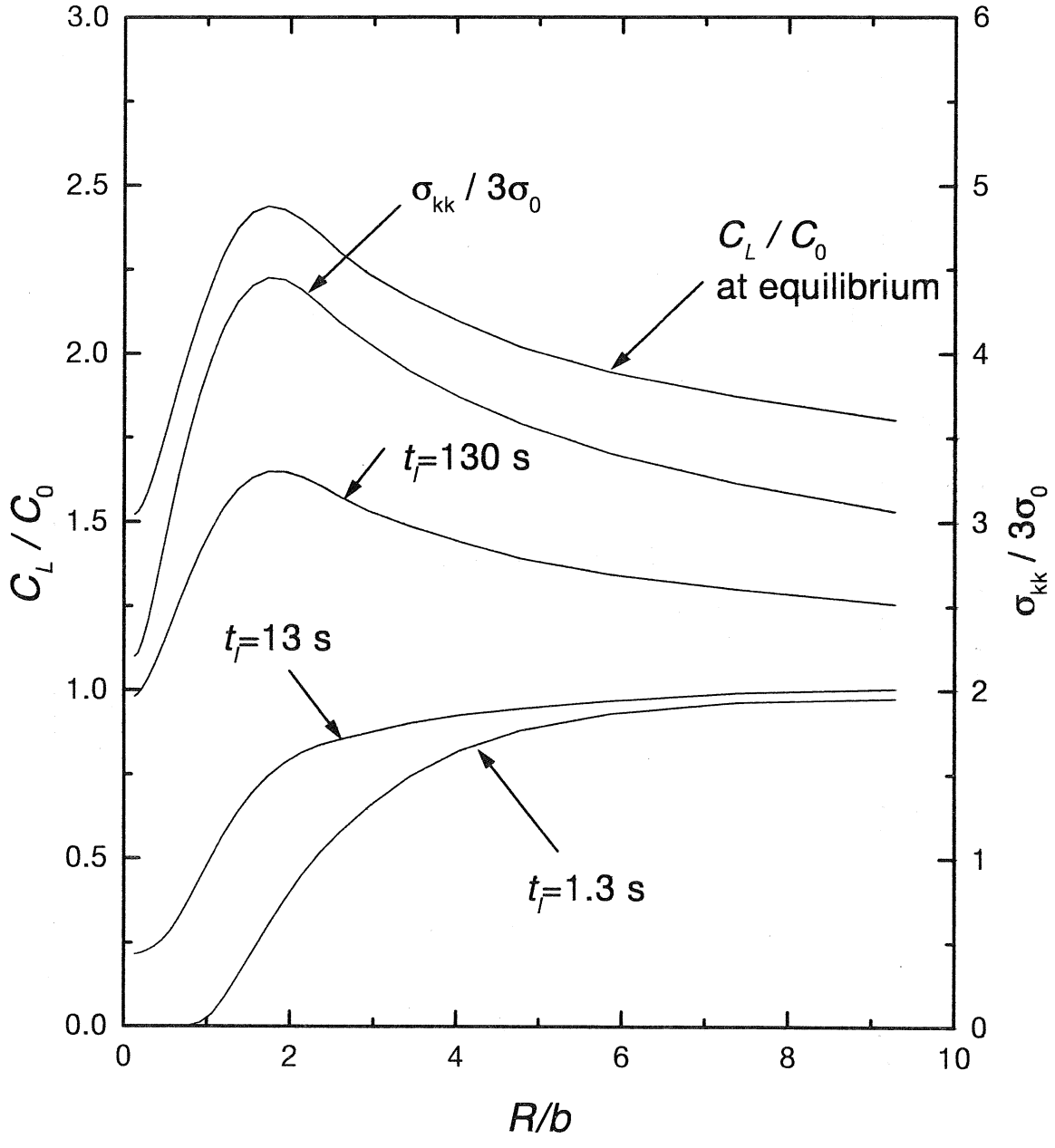

Figure 6 Plot of hydrogen concentration C_L/C_0 in NILS and hydrostatic stress $\sigma_{kk}/3\sigma_0$ vs distance R/b for low strength steel ($\sigma_0 = 250\,\mathrm{MPa}$) at a blunting crack tip upon the completion of loading and at equilibrium (neutralized chemical potential gradients) under zero flux boundary conditions. The load times were $t_l = 1.3, 13, 130\,\mathrm{s}$ and the corresponding crack opening displacement b was $5b_0$. The initial concentration C_0 equals 2.084×10^{21} hydrogen atoms per m^3.

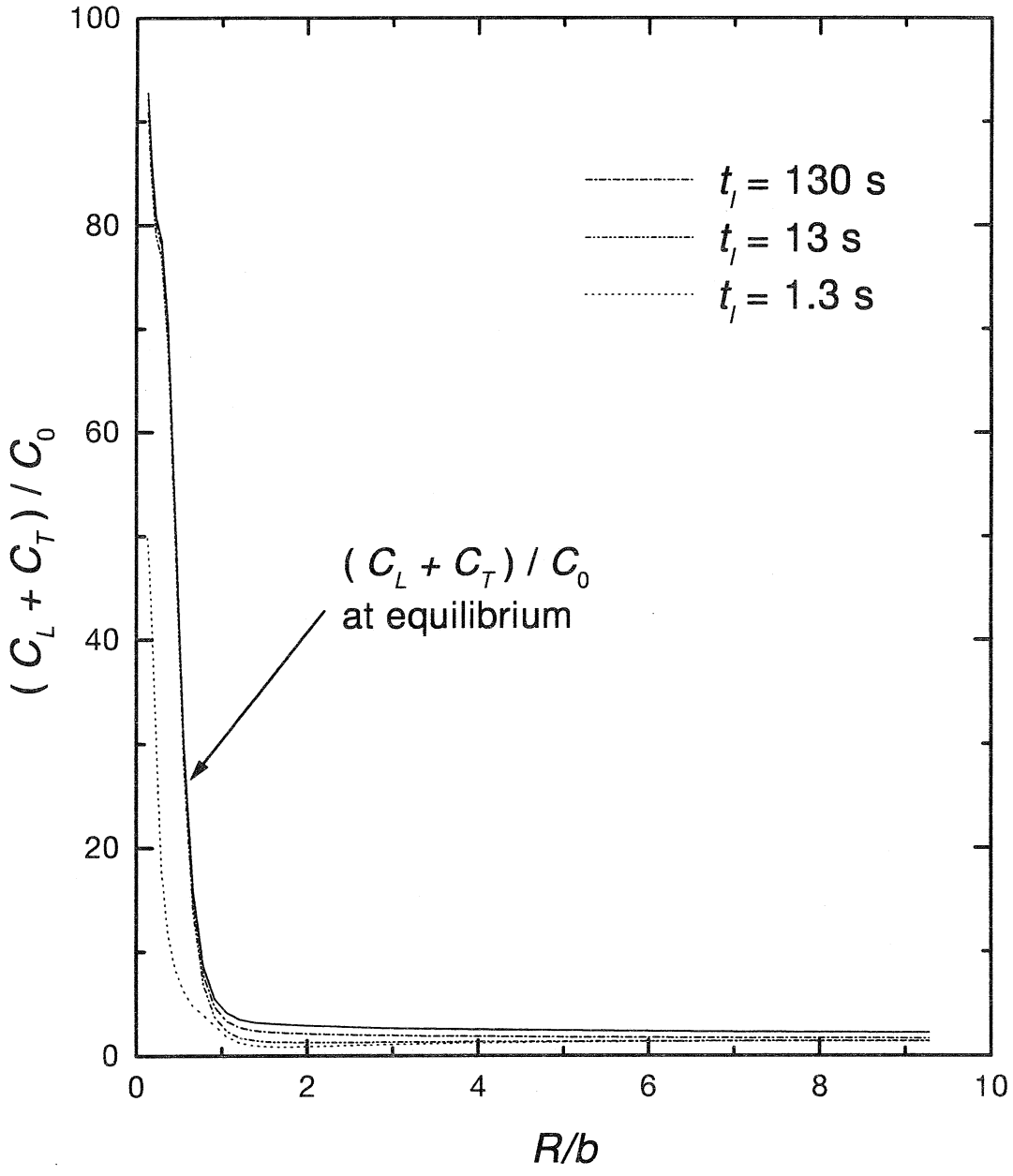

Figure 7 Plot of total hydrogen concentration $(C_L + C_T)/C_0$ vs distance R/b for low strength steel ($\sigma_0 = 250\,\mathrm{MPa}$) at a blunting crack tip upon the completion of loading and at equilibrium (neutralized chemical potential gradients) under zero flux boundary conditions. The load times were $t_l = 1.3, 13, 130\mathrm{s}$ and the corresponding crack opening displacement b was $5b_0$. The initial concentration C_0 equals 2.084×10^{21} hydrogen atoms per m^3.

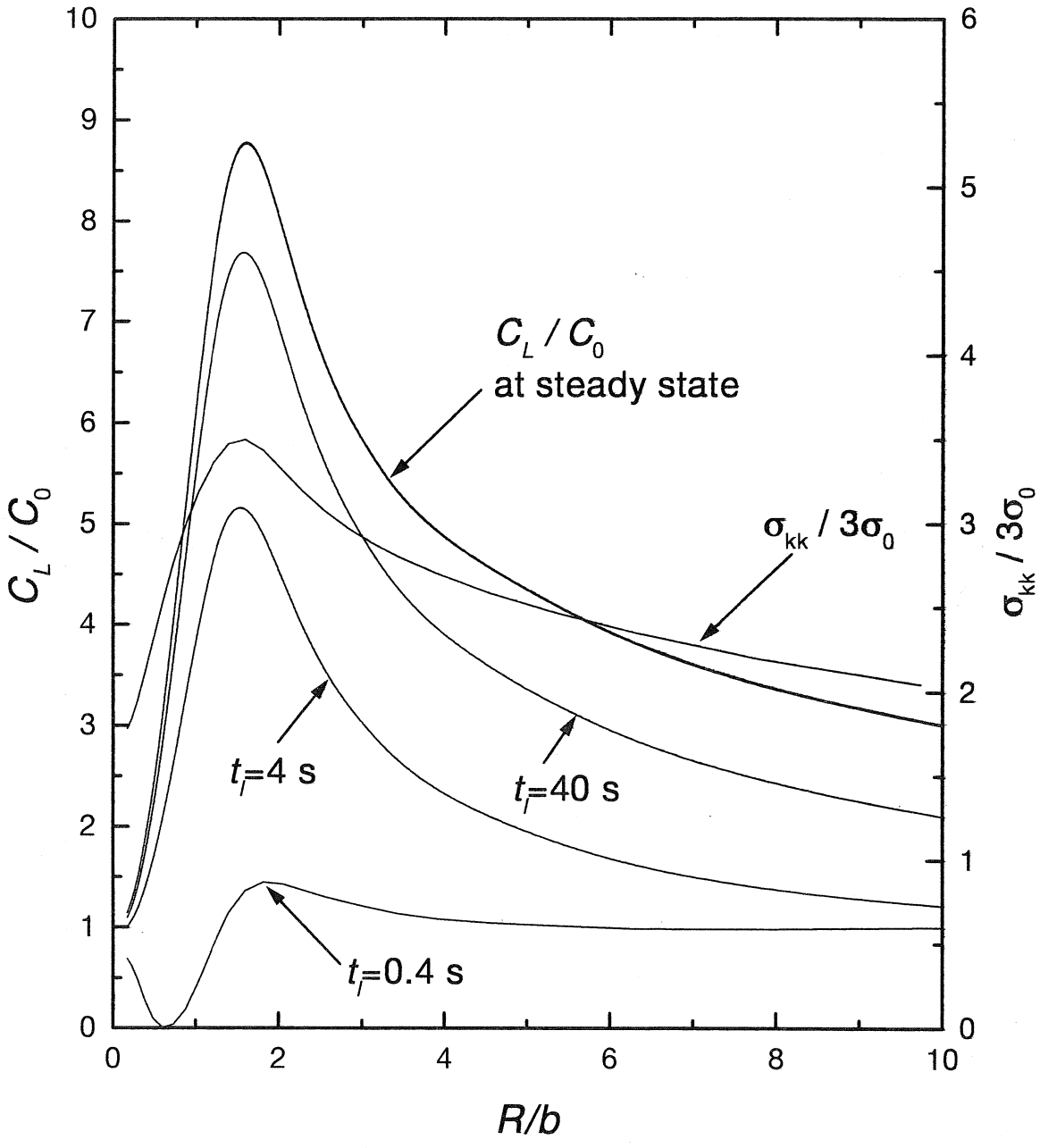

Figure 8 Plot of hydrogen concentration C_L/C_0 in NILS and hydrostatic stress $\sigma_{kk}/3\sigma_0$ vs distance R/b for high strength steel ($\sigma_0 = 1200\text{MPa}$) at a blunting crack tip upon the completion of loading and at steady state under constant concentration boundary conditions. The load times were $t_l = 0.4, 4, 40\text{s}$ and the corresponding crack opening displacement b was $3.5\,b_0$. The initial concentration C_0 equals 2.084×10^{21} hydrogen atoms per m^3.

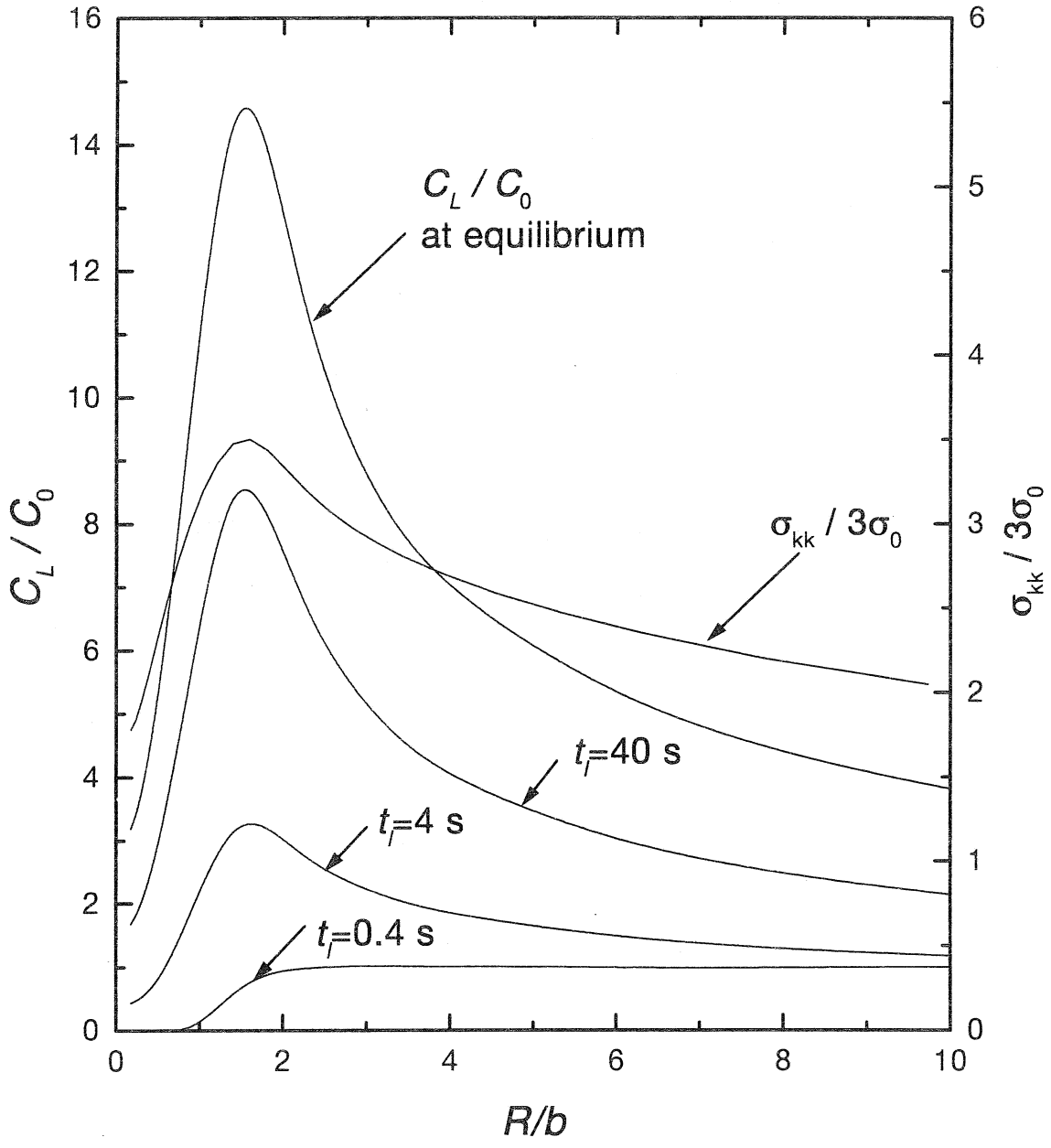

Figure 9 Plot of hydrogen concentration C_L/C_0 in NILS and hydrostatic stress $\sigma_{kk}/3\sigma_0$ vs distance R/b for high strength steel ($\sigma_0 = 1200\text{MPa}$) at a blunting crack tip upon the completion of loading and at equilibrium (neutralized chemical potential gradients) under zero flux boundary conditions. The load times were $t_l = 0.4, 4, 40\text{s}$ and the corresponding crack opening displacement b was $3.5\,b_0$. The initial concentration C_0 equals 2.084×10^{21} hydrogen atoms per m^3.

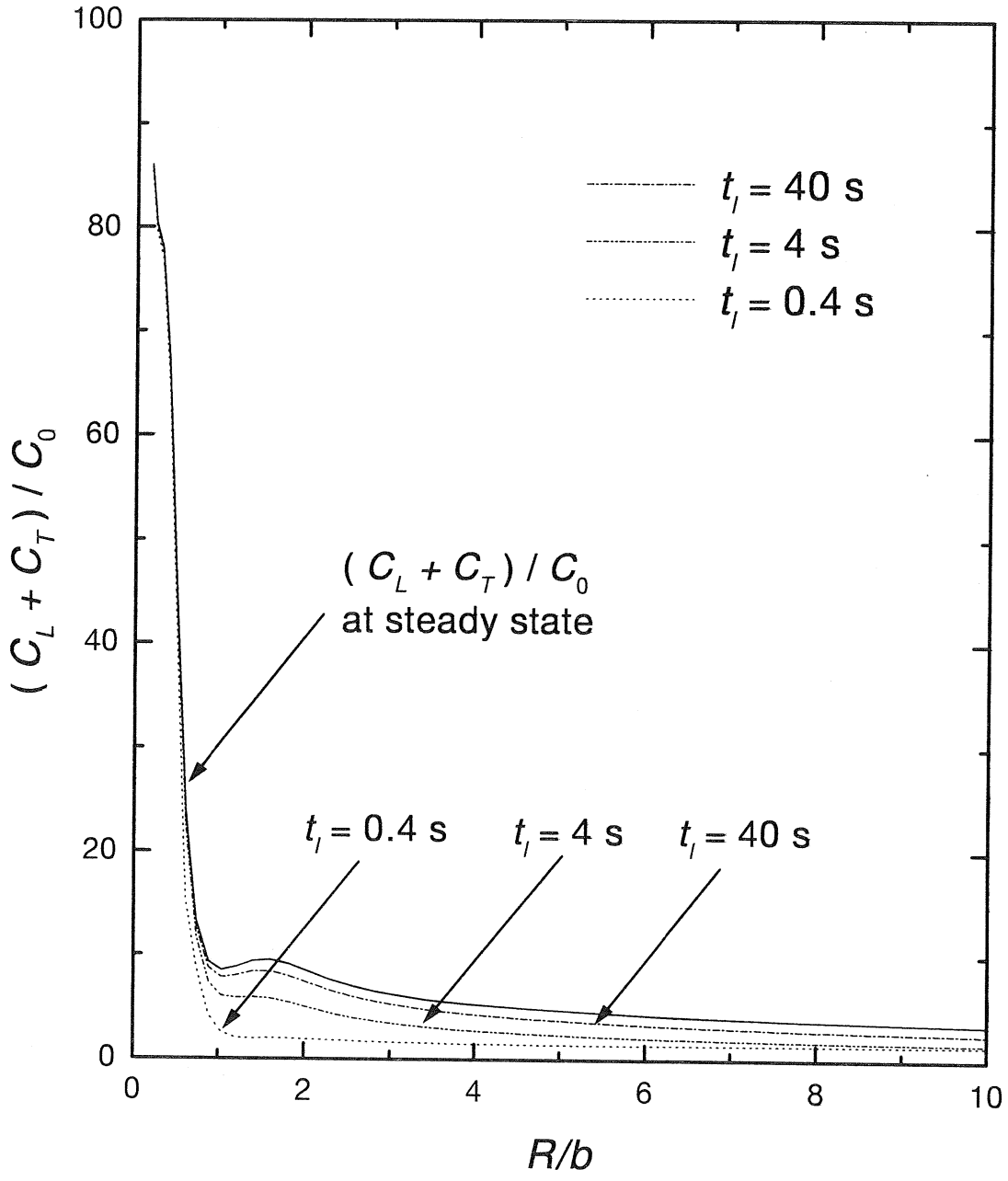

Figure 10 Plot of total hydrogen concentration $(C_L + C_T)/C_0$ **vs distance** R/b **for high strength steel** ($\sigma_0 = 1200\text{MPa}$) **at a blunting crack tip upon the completion of loading and at steady state under constant concentration boundary conditions. The load times were** $t_l = 0.4, 4, 40\text{s}$ **and the corresponding crack opening displacement** b **was** $3.5\,b_0$. **The initial concentration** C_0 **equals** 2.084×10^{21} **hydrogen atoms per** m^3.

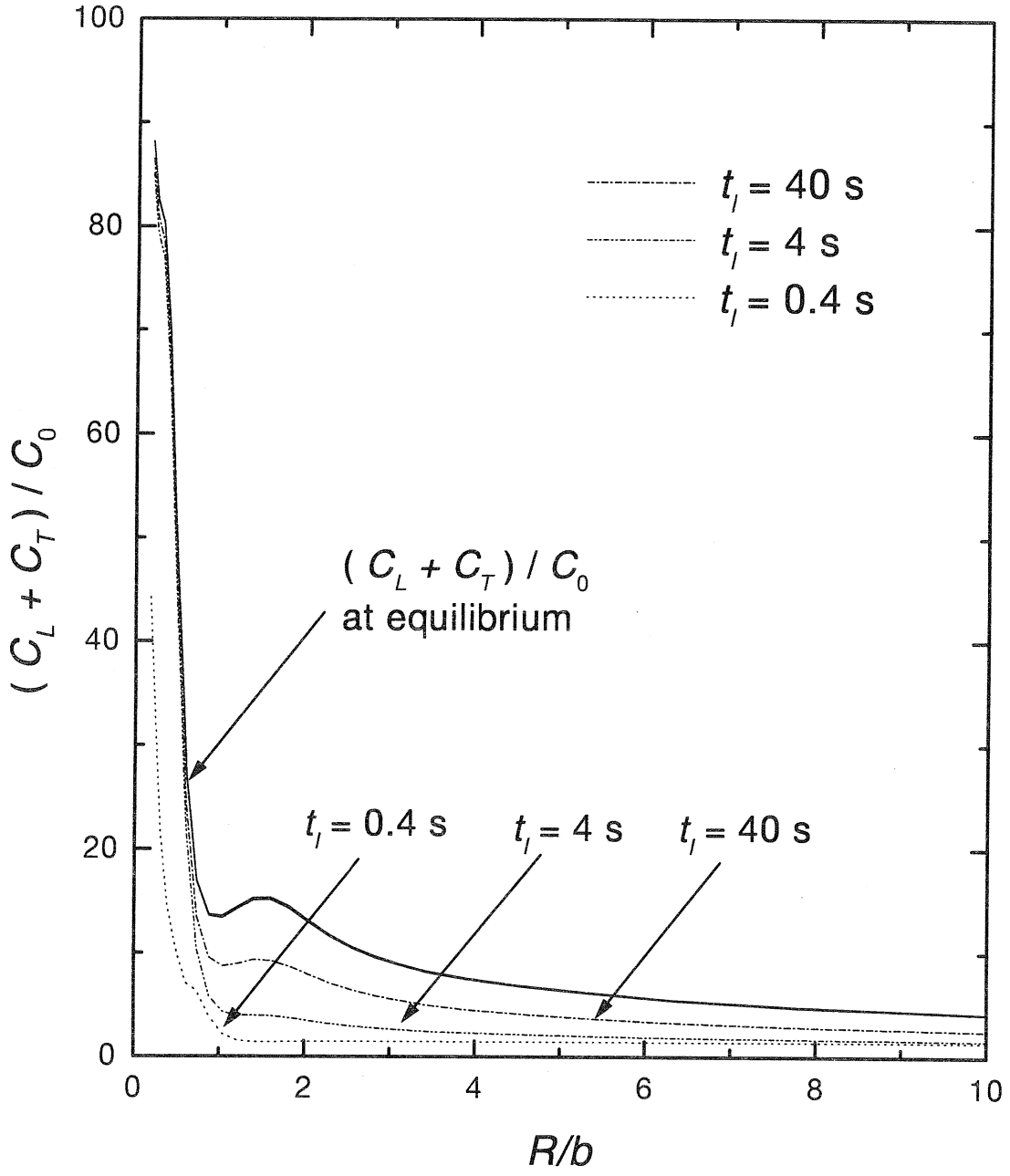

Figure 11 Plot of total hydrogen concentration $(C_L + C_T)/C_0$ vs distance R/b for high strength steel ($\sigma_0 = 250\,\mathrm{MPa}$) at a blunting crack tip upon the completion of loading and at equilibrium (neutralized chemical potential gradients) under zero flux boundary conditions. The load times were $t_l = 0.4, 4, 40\,\mathrm{s}$ and the corresponding crack opening displacement b was $3.5\,b_0$. The initial concentration C_0 equals 2.084×10^{21} hydrogen atoms per m^3.

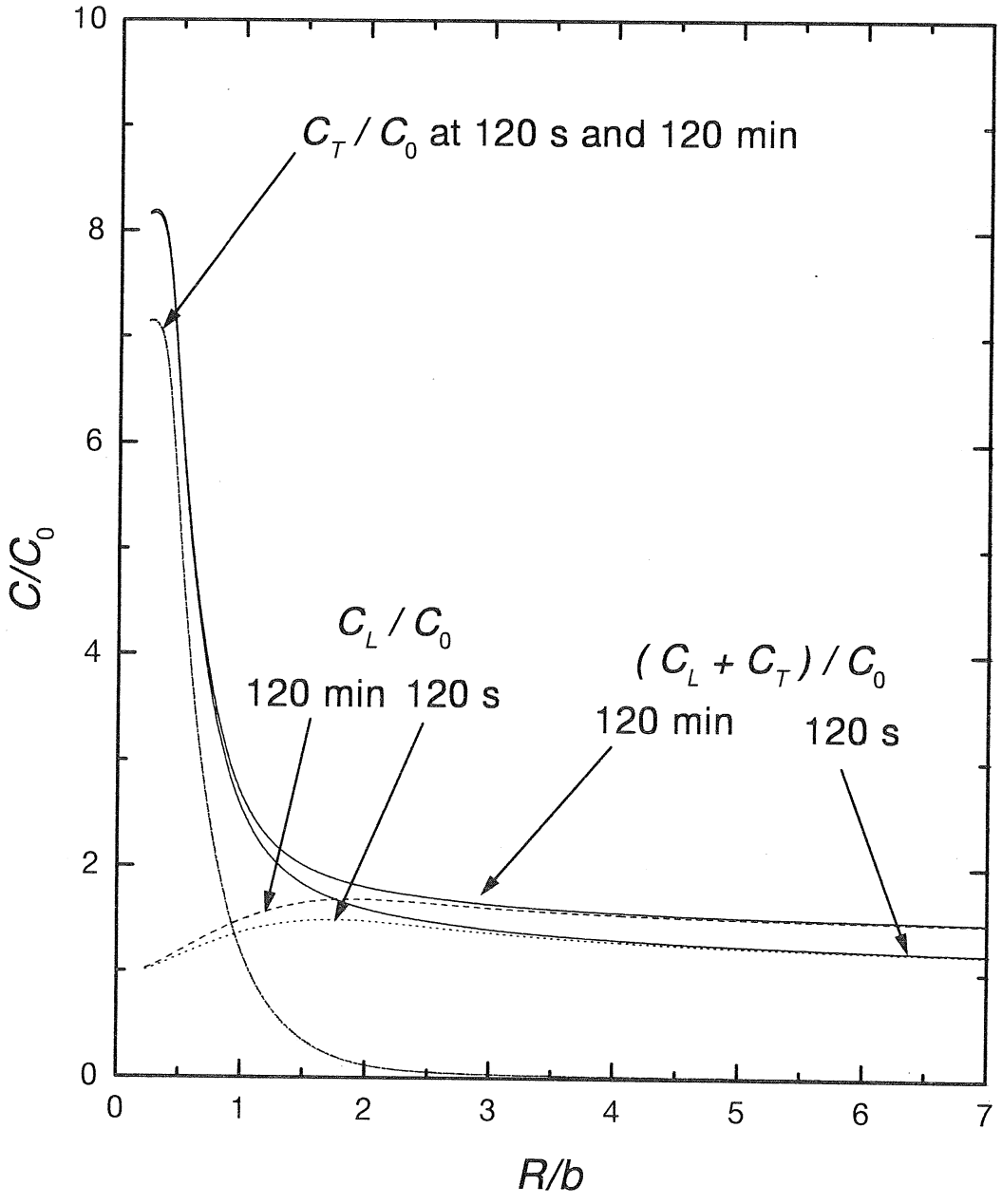

Figure 12 Plot of hydrogen concentration C_L/C_0 in NILS, C_T/C_0 in trapping sites and $(C_L + C_T)/C_0$ vs the normalized distance R/b in front of a blunting crack tip in niobium ($\sigma_0 = 250\,\mathrm{MPa}$) upon the completion of loading at time $t_l = 120\mathrm{s}$ and after 120m, when the crack opening displacement b equals $2.6\,b_0$, and under constant concentration boundary conditions. The initial NILS concentration C_L^0/N_L equals 10^{-4} hydrogen atoms per metal atom.

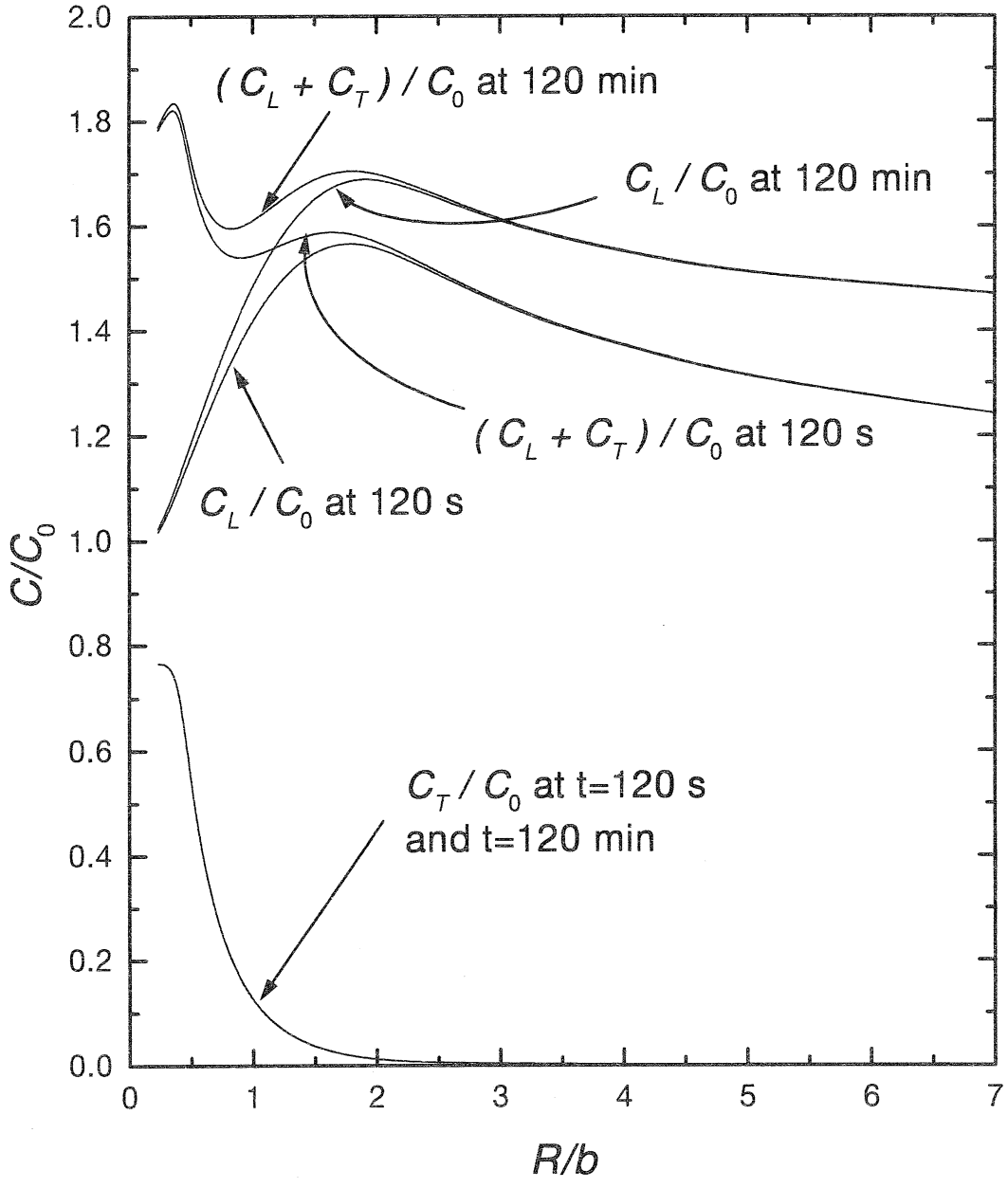

Figure 13 Plot of hydrogen concentration C_L/C_0 in NILS, C_T/C_0 in trapping sites and $(C_L + C_T)/C_0$ vs the normalized distance $^{R/b}$ in front of a blunting crack tip in niobium ($\sigma_0 = 250\,\mathrm{MPa}$) upon the completion of loading at time $t_l = 120\mathrm{s}$ and after 120m, when the crack opening displacement b equals $2.6\,b_0$, and under constant concentration boundary conditions. The initial NILS concentration C_L^0/N_L equals 10^{-3} hydrogen atoms per metal atom.

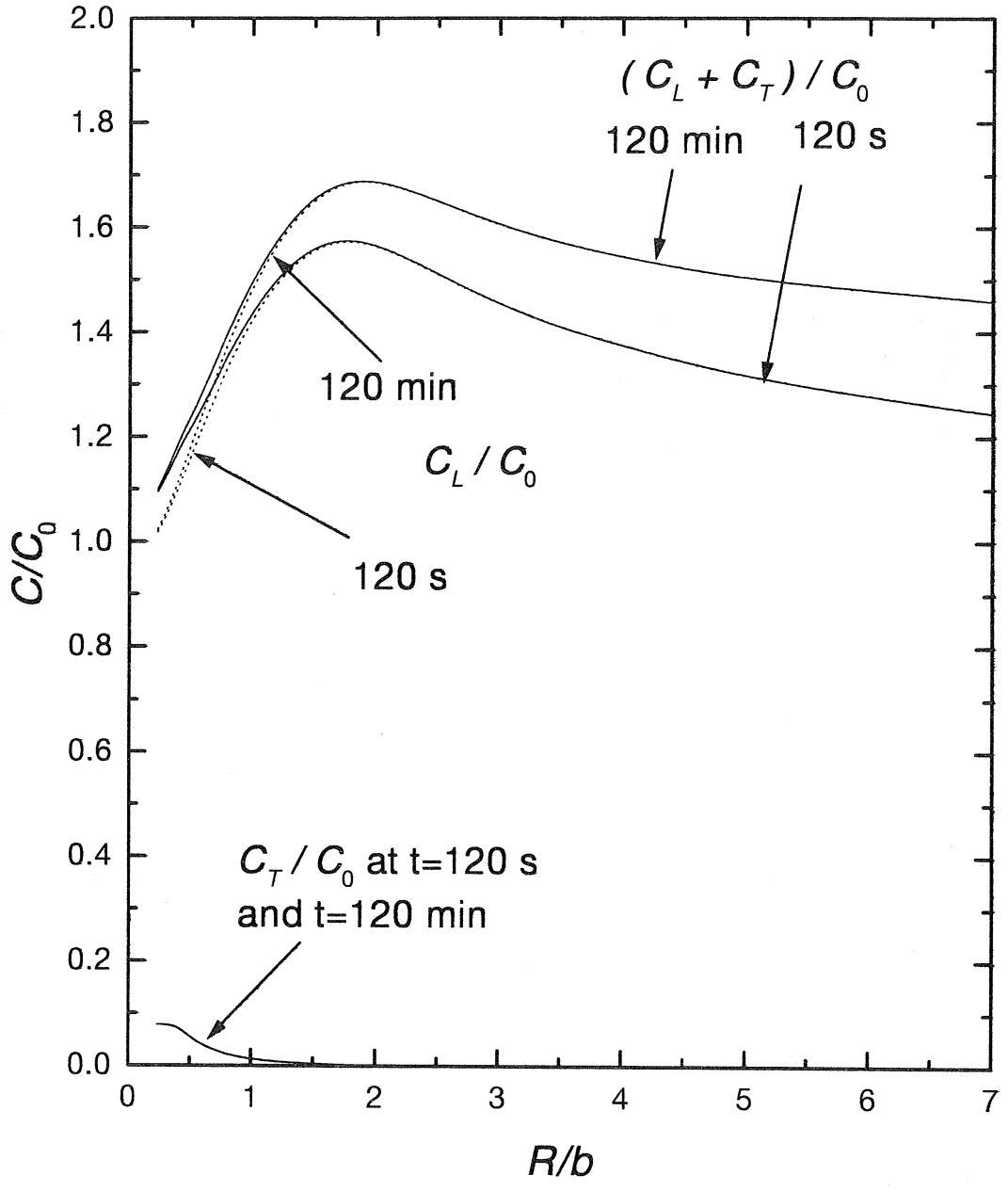

Figure 14 Plot of hydrogen concentration C_L/C_0 in NILS, C_T/C_0 in trapping sites and $(C_L+C_T)/C_0$ vs the normalized distance R/b in front of a blunting crack tip in niobium ($\sigma_0 = 250\,\mathrm{MPa}$) upon the completion of loading at time $t_l = 120\mathrm{s}$ and after 120m, when the crack opening displacement b equals $2.6\,b_0$, and under constant concentration boundary conditions. The initial NILS concentration C_L^0/N_L equals 10^{-2} hydrogen atoms per metal atom.

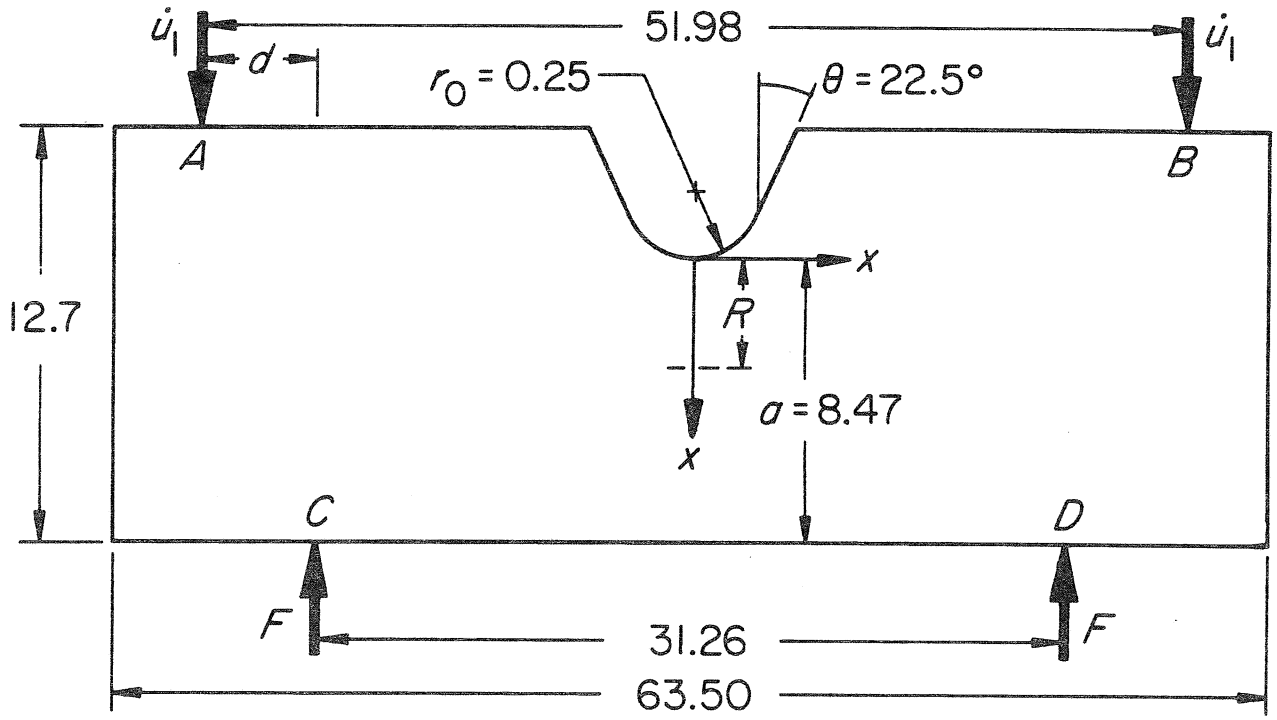

Figure 15 Loading and specimen geometry for rounded notch bend specimen; All dimensions are in mm.

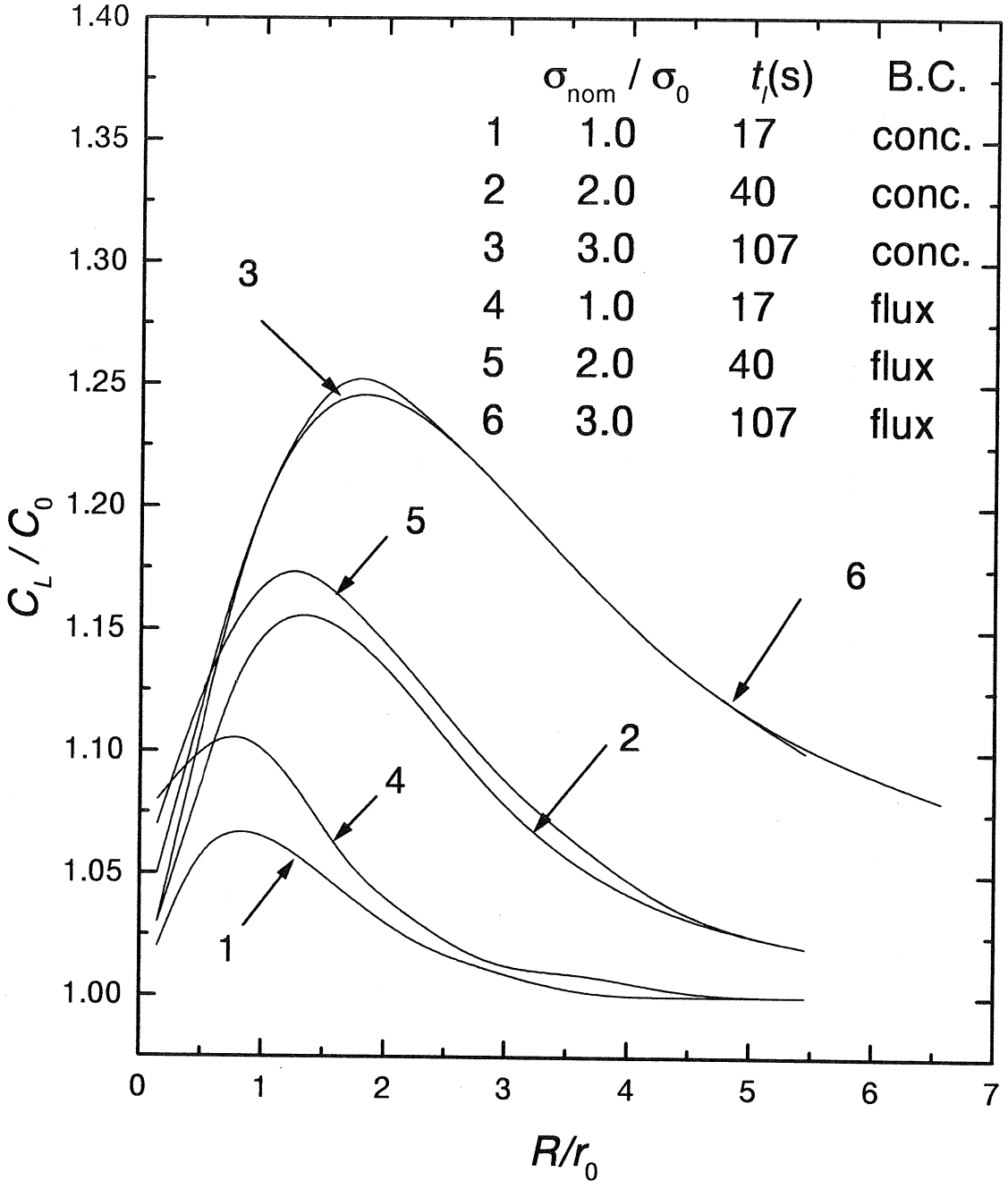

Figure 16 Plot of hydrogen concentration C_L/C_0 in NILS vs normalized distance R/r_0 from the rounded-notch tip in low strength steel ($\sigma_0 = 250\,MPa$) at the end of loading at time t_l with corresponding nominal stress σ_{nom}/σ_0 for both constant concentration and zero flux boundary conditions. Initial concentration C_0 equals 2.084×10^{21} hydrogen atoms per m^3.

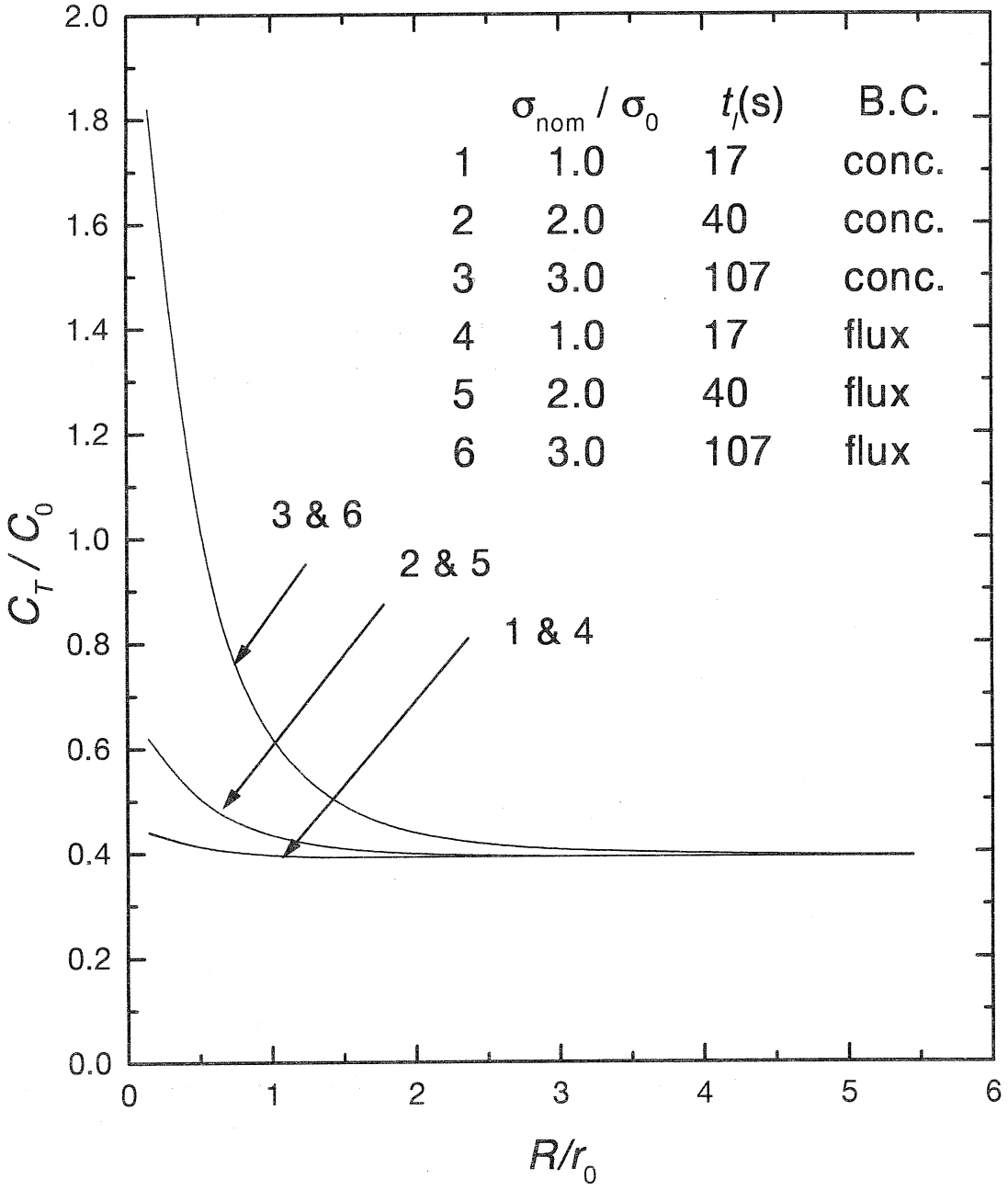

Figure 17 Plot of hydrogen concentration C_T/C_0 in trapping sites vs normalized distance R/r_0 from the rounded-notch tip in low strength steel ($\sigma_0 = 250\,MPa$) at the end of loading at time t_l with corresponding nominal stress σ_{nom}/σ_0 for both constant concentration and zero flux boundary conditions. Initial concentration C_0 equals 2.084×10^{21} hydrogen atoms per m^3.

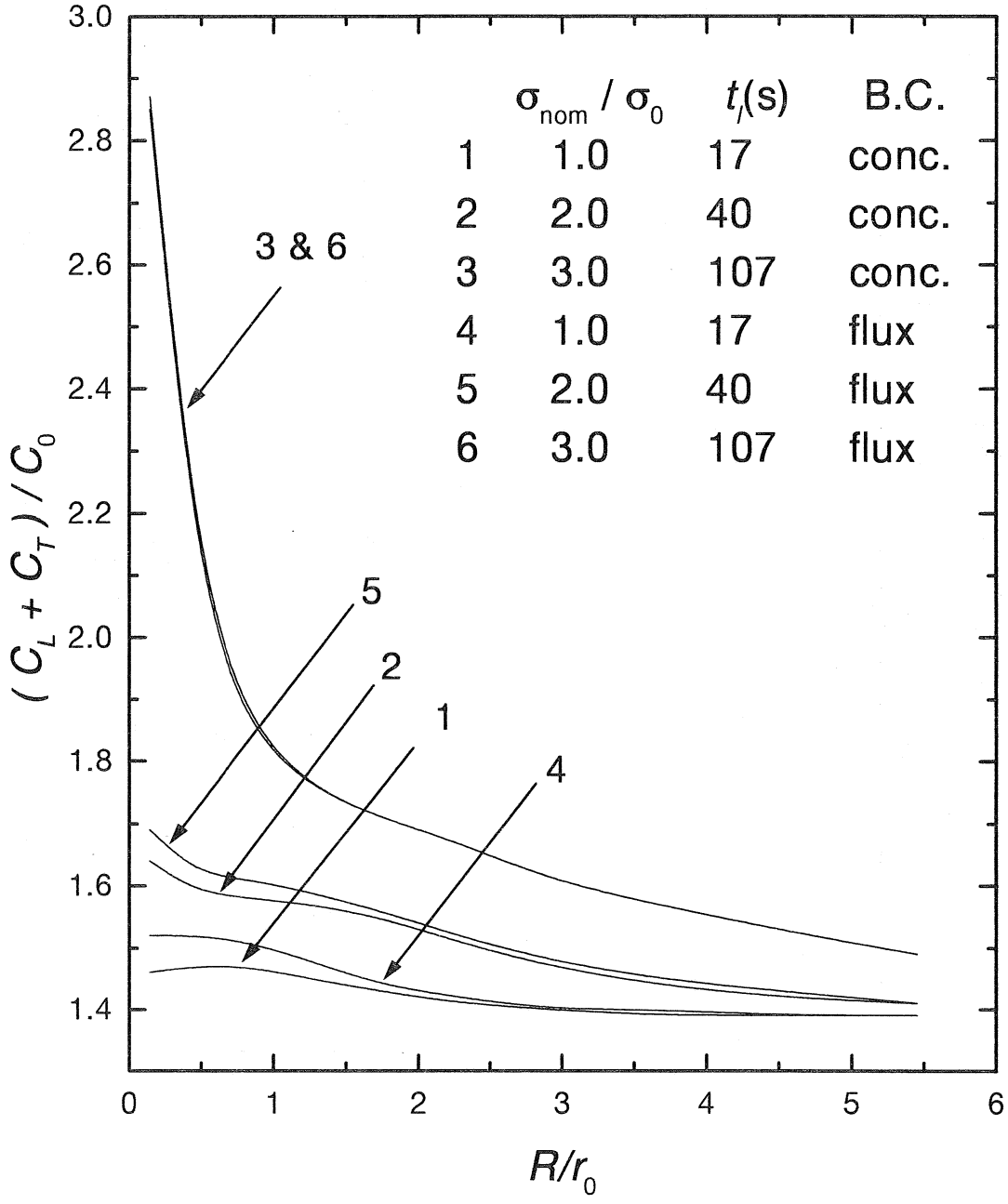

Figure 18 Plot of total hydrogen concentration $(C_L + C_T)/C_0$ vs normalized distance R/r_0 from the rounded-notch tip in low strength steel ($\sigma_0 = 250\,MPa$) at the end of loading at time t_l with corresponding nominal stress σ_{nom}/σ_0 for both constant concentration and zero flux boundary conditions. Initial concentration C_0 equals 2.084×10^{21} hydrogen atoms per m^3.

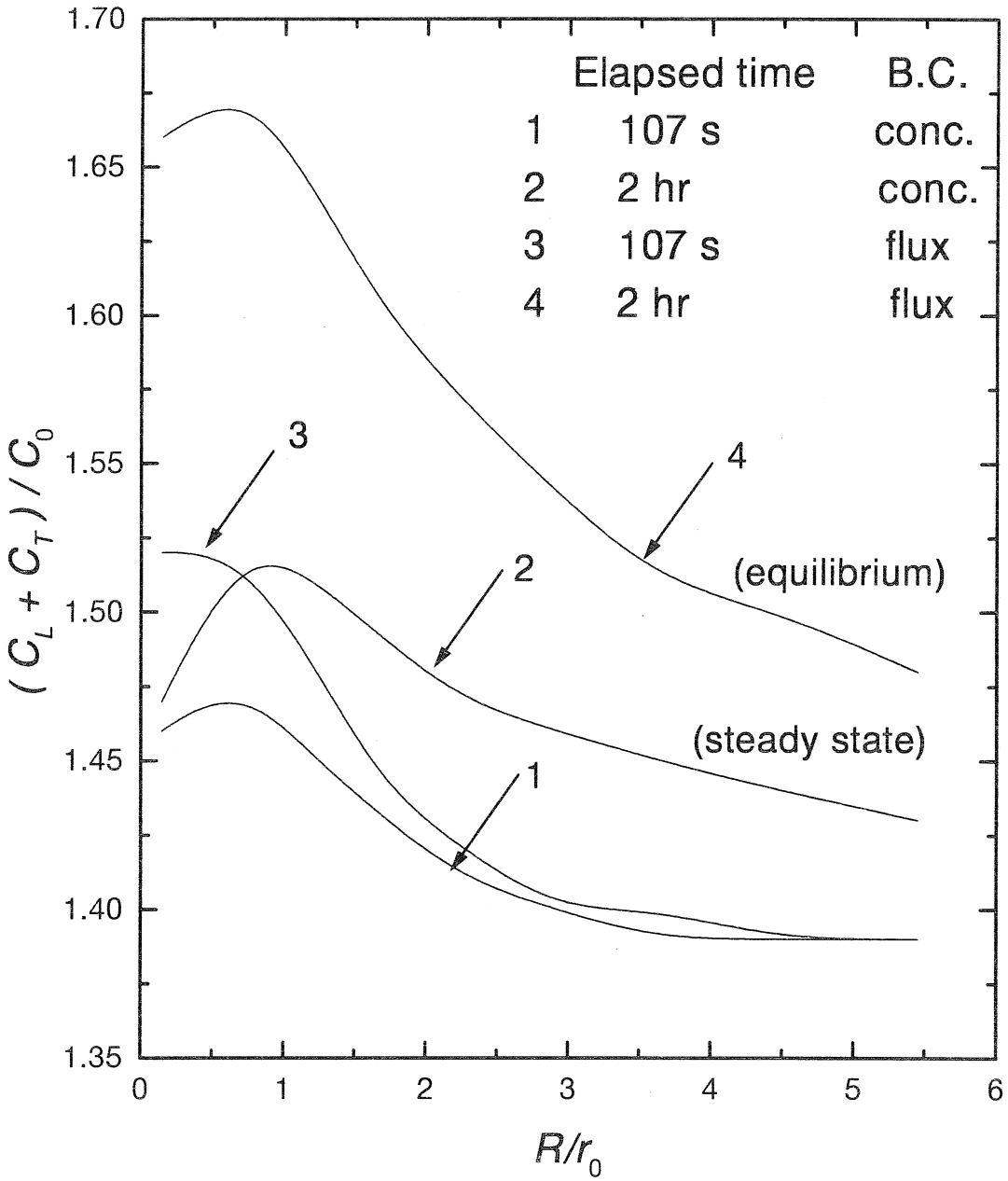

Figure 19 Plot of total hydrogen concentration $(C_L + C_T)/C_0$ vs normalized distance R/r_0 from the rounded-notch tip in low strength steel ($\sigma_0 = 250\,MPa$) at the end of loading at time t_l at which the nominal stress σ_{nom}/σ_0 is equal to 1.0 for both constant concentration and zero flux boundary conditions. Also shown are the corresponding steady state and equilibrium concentrations while loads are held constant at $\sigma_{nom}/\sigma_0 = 1.0$.

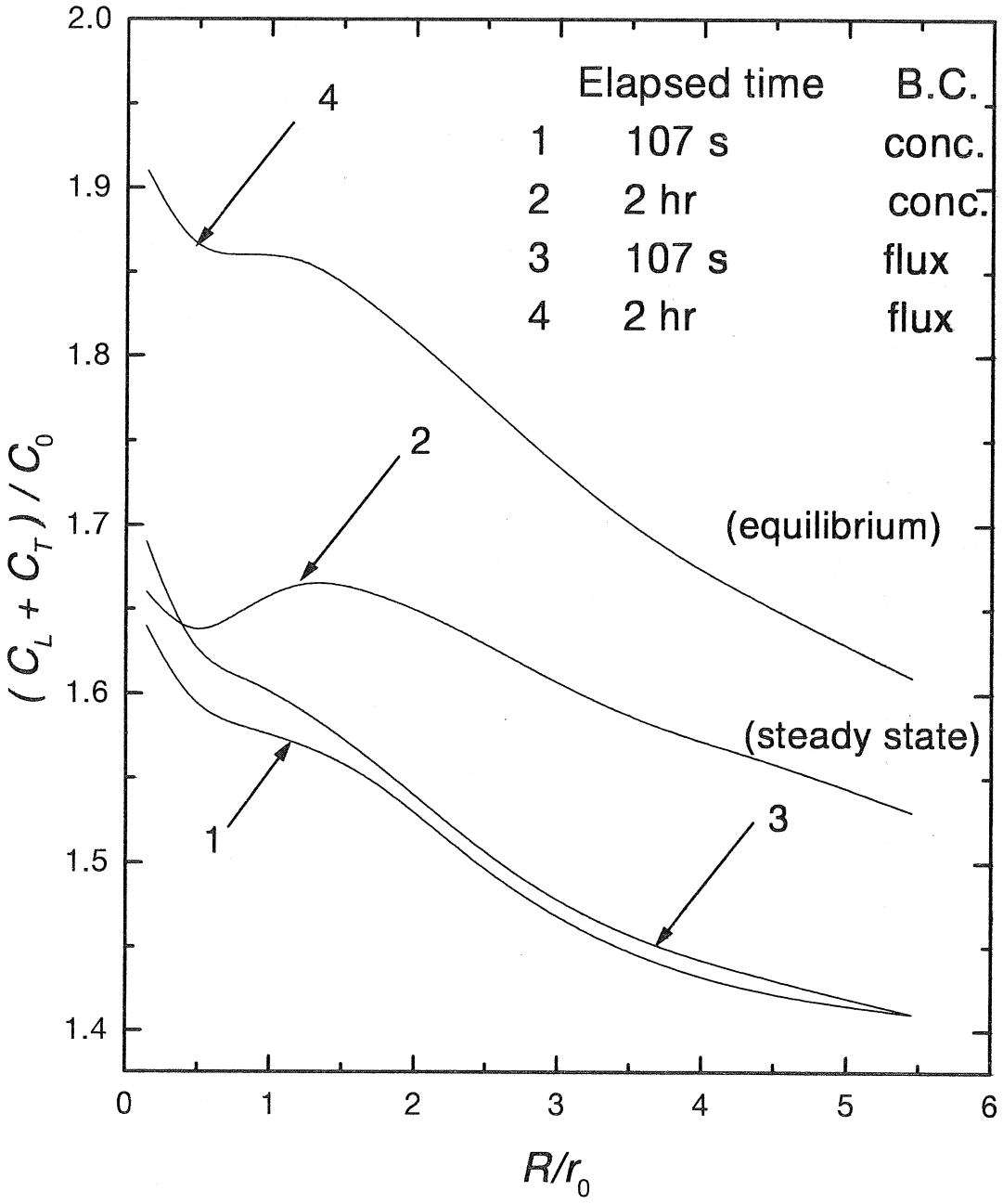

Figure 20 Plot of total hydrogen concentration $(C_L + C_T)/C_0$ vs normalized distance R/r_0 from the rounded-notch tip in low strength steel ($\sigma_0 = 250\,MPa$) at the end of loading at time t_l at which the nominal stress σ_{nom}/σ_0 is equal to 2.0 for both constant concentration and zero flux boundary conditions. Also shown are the corresponding steady state and equilibrium concentrations while loads are held constant at $\sigma_{nom}/\sigma_0 = 2.0$.

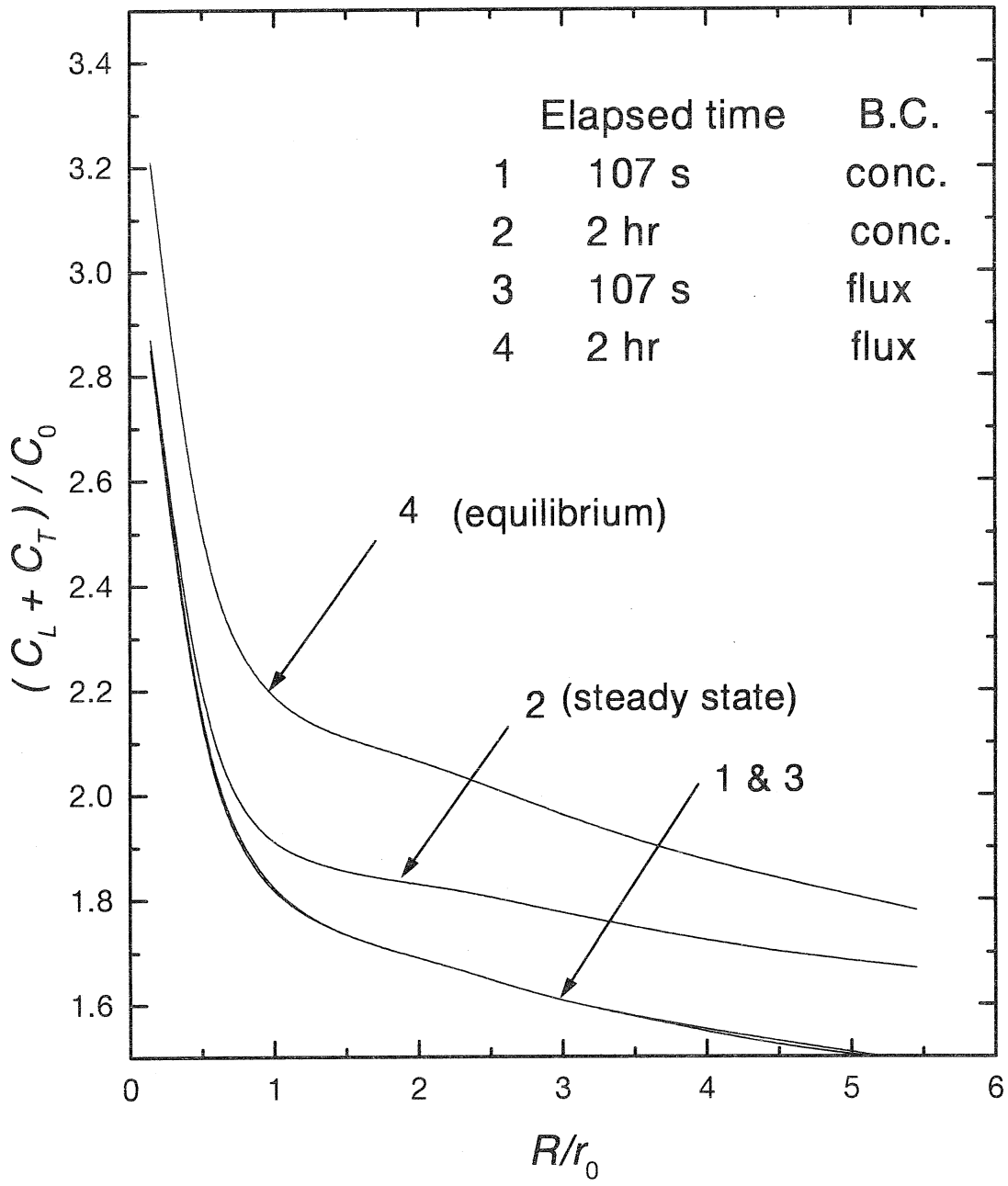

Figure 21 Plot of total hydrogen concentration $(C_L + C_T)/C_0$ vs normalized distance R/r_0 from the rounded-notch tip in low strength steel ($\sigma_0 = 250\,MPa$) at the end of loading at time t_l at which the nominal stress σ_{nom}/σ_0 is equal to 3.0 for both constant concentration and zero flux boundary conditions. Also shown are the corresponding steady state and equilibrium concentrations while loads are held constant at $\sigma_{nom}/\sigma_0 = 3.0$.

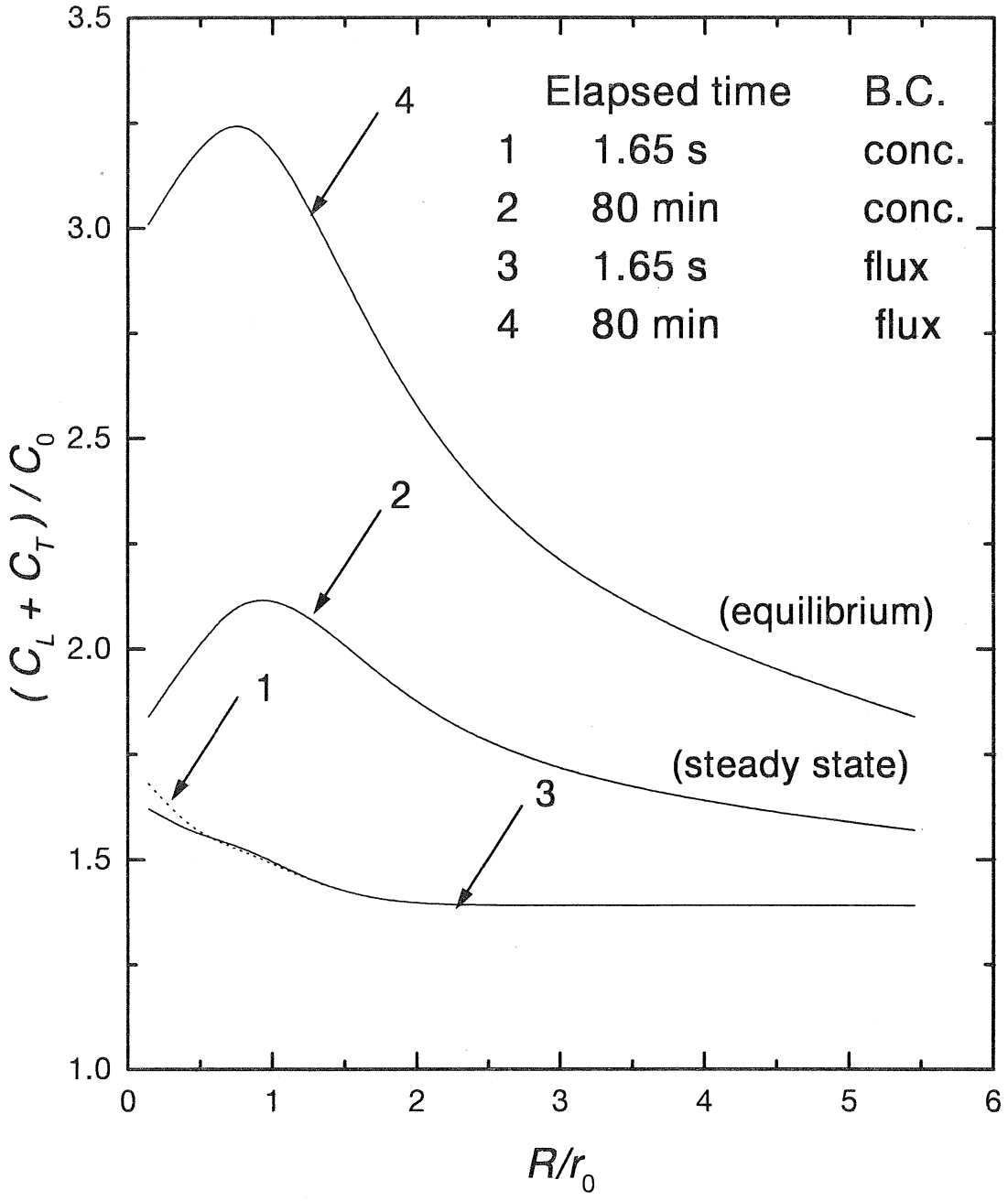

Figure 22 Plot of total hydrogen concentration $(C_L + C_T)/C_0$ vs normalized distance R/r_0 from the rounded-notch tip in high strength steel ($\sigma_0 = 1200\text{MPa}$) at the end of loading at time t_l at which the nominal stress σ_{nom}/σ_0 is equal to 1.0 for both constant concentration and zero flux boundary conditions. Also shown are the corresponding steady state and equilibrium concentrations while loads are held constant at $\sigma_{nom}/\sigma_0 = 1.0$.

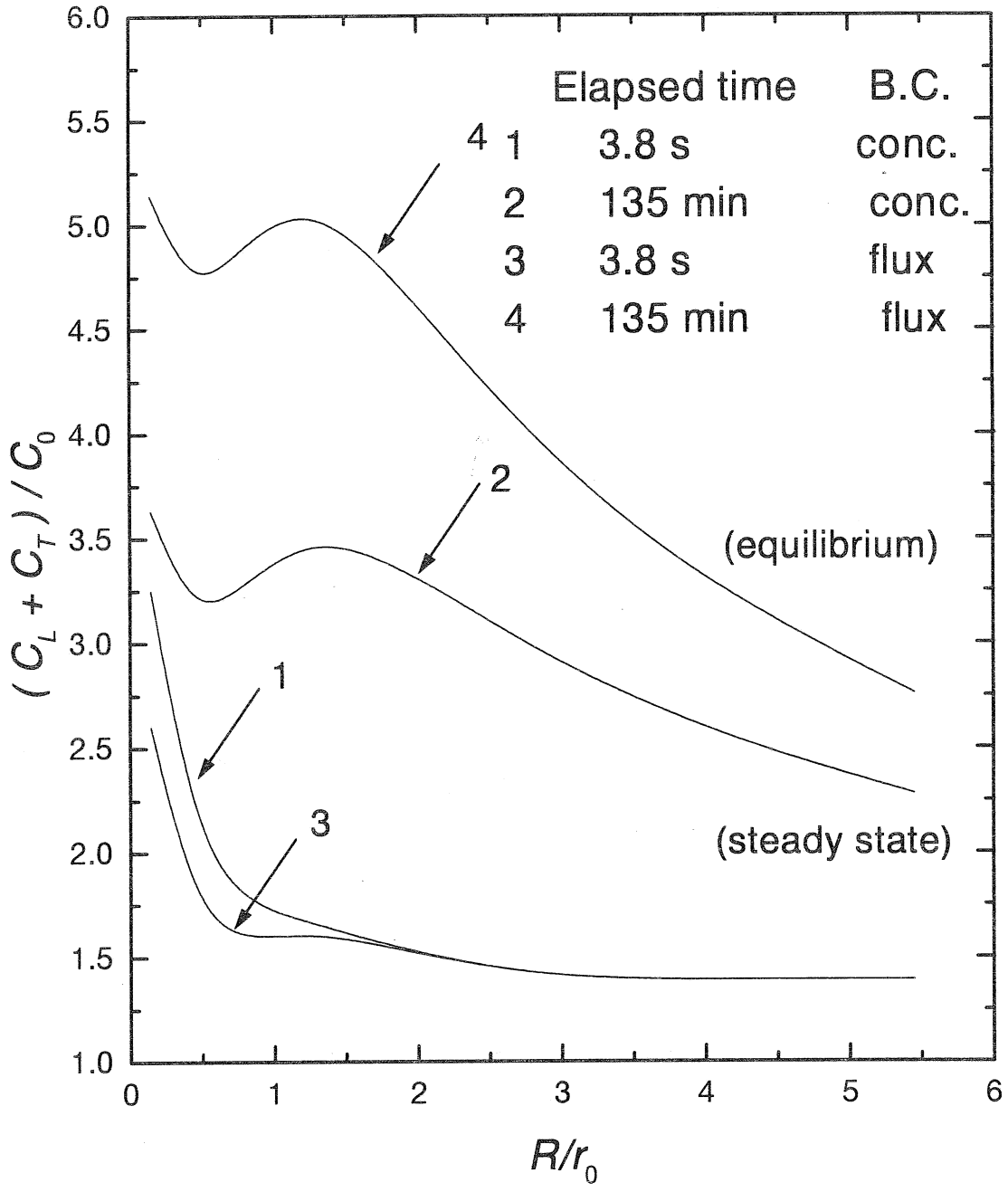

Figure 23 Plot of total hydrogen concentration $(C_L + C_T)/C_0$ vs normalized distance R/r_0 from the rounded-notch tip in high strength steel ($\sigma_0 = 1200\text{MPa}$) at the end of loading at time t_l at which the nominal stress σ_{nom}/σ_0 is equal to 2.0 for both constant concentration and zero flux boundary conditions. Also shown are the corresponding steady state and equilibrium concentrations while loads are held constant at $\sigma_{nom}/\sigma_0 = 2.0$.

List of Recent TAM Reports

No.	Authors	Title	Date
809	Xin, Y.-B., and K. J. Hsia	Simulation of the brittle–ductile transition in silicon single crystals using dislocation mechanics—*Acta Metallurgica et Materialia* **45**, 1747–1759 (1997)	Oct. 1995
810	Ulysse, P., and R. E. Johnson	A plane-strain upper-bound analysis of unsymmetrical single-hole and multi-hole extrusion processes	Oct. 1995
811	Fried, E.	Continua described by a microstructural field—*Zeitschrift für angewandte Mathematik und Physik* **47**, 168–175 (1996)	Nov. 1995
812	Mittal, R., and S. Balachandar	Autogeneration of three-dimensional vortical structures in the near wake of a circular cylinder	Nov. 1995
813	Segev, R., E. Fried, and G. de Botton	Force theory for multiphase bodies—*Journal of Geometry and Physics* **20**, 371–392 (1996)	Dec. 1995
814	Weaver, R. L.	The effect of an undamped finite-degree-of-freedom "fuzzy" substructure: Numerical solutions and theoretical discussion—*Journal of the Acoustical Society of America* **100**, 3159–3164 (1996)	Jan. 1996
815	Haber, R. B., C. S. Jog, and M. P. Bendsøe	A new approach to variable-topology shape design using a constraint on perimeter—*Structural Optimization* **11**, 1–12 (1996)	Feb. 1996
816	Xu, Z.-Q., and K. J. Hsia	A numerical solution of a surface crack under cyclic hydraulic pressure loading—*ASME Journal of Tribology* **119**, 637–645 (1997)	Mar. 1996
817	Adrian, R. J.	Bibliography of particle velocimetry using imaging methods: 1917–1995—*Produced and distributed in cooperation with TSI, Inc., St. Paul, Minn.*	Mar. 1996
818	Fried, E., and G. Grach	An order-parameter based theory as a regularization of a sharp-interface theory for solid–solid phase transitions—*Archive for Rational Mechanics and Analysis* **138**, 355–404 (1997)	Mar. 1996
819	Vonderwell, M. P., and D. N. Riahi	Resonant instability mode triads in the compressible boundary-layer flow over a swept wing—*International Journal of Engineering Science* **36**, 599–624 (1998)	Mar. 1996
820	Short, M., and D. S. Stewart	Low-frequency two-dimensional linear instability of plane detonation—*Journal of Fluid Mechanics* **340**, 249–295 (1997)	Mar. 1996
821	Casagranda, A., and P. Sofronis	On the scaling laws for the consolidation of nanocrystalline powder compacts—Proceedings of the *IUTAM Symposium on the Mechanics of Granular and Porous Materials*, N. A. Fleck and A. C. F. Cocks, eds. The Netherlands: Kluwer Academic Publishers, 105–116 (1997)	Apr. 1996
822	Xu, S., and D. S. Stewart	Deflagration-to-detonation transition in porous energetic materials: A comparative model study—*Journal of Engineering Mathematics* **31**, 143–172 (1997)	Apr. 1996
823	Weaver, R. L.	Mean and mean-square responses of a prototypical master/fuzzy structure—*Journal of the Acoustical Society of America* **101**, 1441–1449 (1997)	Apr. 1996
824	Fried, E.	Correspondence between a phase-field theory and a sharp-interface theory for crystal growth—*Continuum Mechanics and Thermodynamics* **9**, 33–60 (1997)	Apr. 1996
825	Students in TAM 293–294	Thirty-third student symposium on engineering mechanics, J. W. Phillips, coordinator: Selected senior projects by W. J. Fortino II, A. A. Mordock, and M. R. Sawicki	May 1996
826	Riahi, D. N.	Effects of roughness on nonlinear stationary vortices in rotating disk flows—*Mathematical and Computer Modeling* **25**, 71–82 (1997)	June 1996
827	Riahi, D. N.	Nonlinear instabilities of shear flows over rough walls, *Far East Journal of Applied Mathematics*, in press (1998)	June 1996
828	Weaver, R. L.	Multiple scattering theory for a plate with sprung masses, mean responses—*Journal of the Acoustical Society of America* **101**, 3466–3414 (1997)	July 1996
829	Moser, R. D., M. M. Rogers, and D. W. Ewing	Self-similarity of time-evolving plane wakes *Journal of Fluid Mechanics*, in press (1998)	July 1996

List of Recent TAM Reports (cont'd)

No.	Authors	Title	Date
830	Lufrano, J. M., and P. Sofronis	Enhanced hydrogen concentrations ahead of rounded notches and cracks: Competition between plastic strain and hydrostatic stress—*Acta Metallurgica et Materialia*, in press (1998)	July 1996
831	Riahi, D. N.	Effects of surface corrugation on primary instability modes in wall-bounded shear flows	Aug. 1996
832	Bechel, V. T., and N. R. Sottos	Application of debond length measurements to examine the mechanics of fiber pushout	Aug. 1996
833	Riahi, D. N.	Effect of centrifugal and Coriolis forces on chimney convection during alloy solidification—*Journal of Crystal Growth* **179**, 287–296 (1997)	Sept. 1996
834	Cermelli, P., and E. Fried	The influence of inertia on configurational forces in a deformable solid—*Proceedings of the Royal Society of London A* **453**, 1915–1927 (1997)	Oct. 1996
835	Riahi, D. N.	On the stability of shear flows with combined temporal and spatial imperfections	Oct. 1996
836	Carranza, F. L., B. Fang, and R. B. Haber	An adaptive space–time finite element model for oxidation-driven fracture, *Computer Methods in Applied Mechanics and Engineering*, in press (1997)	Nov. 1996
837	Carranza, F. L., B. Fang, and R. B. Haber	A moving cohesive interface model for fracture in creeping materials, *Computational Mechanics* **19**, 517–521 (1997)	Nov. 1996
838	Balachandar, S., R. Mittal, and F. M. Najjar	Properties of the mean wake recirculation region in two-dimensional bluff body wakes—*Journal of Fluid Mechanics*, in press (1997)	Dec. 1996
839	Ti, B. W., W. D. O'Brien, Jr., and J. G. Harris	Measurements of coupled Rayleigh wave propagation in an elastic plate—*Journal of the Acoustical Society of America* **102**, 1528–1531	Dec. 1996
840	Phillips, W. R. C.	On finite-amplitude rotational waves in viscous shear flows—*Studies in Applied Mathematics* **100**, in press (1998)	Jan. 1997
841	Riahi, D. N.	Direct resonance analysis and modeling for a turbulent boundary layer over a corrugated surface—*Acta Mechanica*, in press (1998)	Jan. 1997
842	Liu, Z.-C., R. J. Adrian, C. D. Meinhart, and W. Lai	Structure of a turbulent boundary layer using a stereoscopic, large format video-PIV—*Developments in Laser Techniques and Fluid Mechanics*, 259–273 (1997)	Jan. 1997
843	Fang, B., F. L. Carranza, and R. B. Haber	An adaptive discontinuous Galerkin method for viscoplastic analysis—*Computer Methods in Applied Mechanics and Engineering* **150**, 191–198 (1997)	Jan. 1997
844	Xu, S., T. D. Aslam, and D. S. Stewart	High-resolution numerical simulation of ideal and non-ideal compressible reacting flows with embedded internal boundaries—*Combustion Theory and Modeling* **1**, 113–142 (1997)	Jan. 1997
845	Zhou, J., C. D. Meinhart, S. Balachandar, and R. J. Adrian	Formation of coherent hairpin packets in wall turbulence—In *Self-Sustaining Mechanisms in Wall Turbulence*, R. L. Panton, ed. Southampton, UK: Computational Mechanics Publications, 109–134 (1997)	Feb. 1997
846	Lufrano, J. M., P. Sofronis, and H. K. Birnbaum	Elastoplastically accommodated hydride formation and embrittlement—*Journal of Mechanics and Physics of Solids*, in press (1998)	Feb. 1997
847	Keane, R. D., N. Fujisawa, and R. J. Adrian	Unsteady non-penetrative thermal convection from non-uniform surfaces—In *Geophysical and Astrophysical Convection*, R. Kerr, ed. (1997)	Feb. 1997
848	Aref, H., and M. Brøns	On stagnation points and streamline topology in vortex flows—*Journal of Fluid Mechanics* **370**, 1–27 (1998)	Mar. 1997
849	Asghar, S., T. Hayat, and J. G. Harris	Diffraction by a slit in an infinite porous barrier—*Wave Motion*, in press (1998)	Mar. 1997
850	Shawki, T. G., H. Aref, and J. W. Phillips	Mechanics on the Web—Proceedings of the International Conference on Engineering Education (Aug. 1997, Chicago)	Apr. 1997

No.	Authors	Title	Date
851	Stewart, D. S., and J. Yao	The normal detonation shock velocity–curvature relationship for materials with non-ideal equation of state and multiple turning points—*Combustion and Flame*, in press (1998)	Apr. 1997
852	Fried, E., A. Q. Shen, and S. T. Thoroddsen	Wave patterns in a thin layer of sand within a rotating horizontal cylinder—*Physics of Fluids* **10**, 10–12 (1998)	Apr. 1997
853	Boyland, P. L., H. Aref, and M. A. Stremler	Topological fluid mechanics of stirring	Apr. 1997
854	Parker, S. J., and S. Balachandar	Viscous and inviscid instabilities of flow along a streamwise corner—*Theoretical and Computational Fluid Dynamics*, in press (1997)	May 1997
855	Soloff, S. M., R. J. Adrian, and Z.-C. Liu	Distortion compensation for generalized stereoscopic particle image velocimetry—*Measurement Science and Technology* **8**, 1–14 (1997)	May 1997
856	Zhou, Z., R. J. Adrian, S. Balachandar, and T. M. Kendall	Mechanisms for generating coherent packets of hairpin vortices in near-wall turbulence—*Journal of Fluid Mechanics*, in press (1997)	June 1997
857	Neishtadt, A. I., D. L. Vainshtein, and A. A. Vasiliev	Chaotic advection in a cubic stokes flow—*Physica D* **111**, 227 (1997).	June 1997
858	Weaver, R. L.	Ultrasonics in an aluminum foam—*Ultrasonics*, in press (1997)	July 1997
859	Riahi, D. N.	High gravity convection in a mushy layer during alloy solidification—In *Nonlinear Instability, Chaos and Turbulence*, D. N. Riahi and L. Debnath, eds., in press (1998)	July 1997
860	Najjar, F. M., and S. Balachandar	Low-frequency unsteadiness in the wake of a normal plate, *Journal of Fluid Mechanics*, in press (1997)	Aug. 1997
861	Short, M.	A parabolic linear evolution equation for cellular detonation instability	Aug. 1997
862	Short, M., and D. S. Stewart	Cellular detonation stability—I: A normal-mode linear analysis	Sept. 1997
863	Carranza, F. L., and R. B. Haber	A numerical study of intergranular fracture and oxygen embrittlement in an elastic–viscoplastic solid—*Journal of the Mechanics and Physics of Solids*, in press (1997)	Oct. 1997
864	Sakakibara, J., and R. J. Adrian	Whole-field measurement of temperature in water using two-color laser-induced fluorescence	Oct. 1997
865	Riahi, D. N.	Effect of surface corrugation on convection in a three-dimensional finite box of fluid-saturated porous material	Oct. 1997
866	Baker, C. F., and D. N. Riahi	Three-dimensional flow instabilities during alloy solidification	Oct. 1997
867	Fried, E.	Introduction (only) to *The Physical and Mathematical Foundations of the Continuum Theory of Evolving Phase Interfaces* (book containing 14 seminal papers dedicated to Morton E. Gurtin), Berlin: Springer-Verlag, in press (1998)	Oct. 1997
868	Folguera, A., and J. G. Harris	Coupled Rayleigh surface waves in a slowly varying elastic waveguide	Oct. 1997
869	Stewart, D. S.	Detonation shock dynamics: Application for precision cutting of metal with detonation waves	Oct. 1997
870	Shrotriya, P., and N. R. Sottos	Creep and relaxation behavior of woven glass/epoxy substrates for multilayer circuit board applications	Nov. 1997
871	Riahi, D. N.	Boundary wave–vortex interaction in channel flow at high Reynolds numbers, *Fluid Dynamics Research*, in press (1998)	Nov. 1997
872	George, W. K., L. Castillo, and M. Wosnik	A theory for turbulent pipe and channel flows—paper presented at *Disquisitiones Mechanicae* (Urbana, Ill., October 1996)	Nov. 1997
873	Aslam, T. D., and D. S. Stewart	Detonation shock dynamics and comparisons with direct numerical simulation	Dec. 1997

List of Recent TAM Reports (cont'd)

No.	Authors	Title	Date
874	Short, M., and A. K. Kapila	Blow-up in semilinear parabolic equations with weak diffusion	Dec. 1997
875	Riahi, D. N.	Analysis and modeling for a turbulent convective plume—*Mathematical and Computer Modeling* **28**, 57–63 (1998)	Jan. 1998
876	Stremler, M. A., and H. Aref	Motion of three point vortices in a periodic parallelogram	Feb. 1998
877	Dey, N., K. J. Hsia, and D. F. Socie	On the stress dependence of high-temperature static fatigue life of ceramics	Feb. 1998
878	Brown, E. N., and N. R. Sottos	Thermoelastic properties of plain weave composites for multilayer circuit board applications	Feb. 1998
879	Riahi, D. N.	On the effect of a corrugated boundary on convective motion	Feb. 1998
880	Riahi, D. N.	On a turbulent boundary layer flow over a moving wavy wall	Mar. 1998
881	Riahi, D. N.	Vortex formation and stability analysis for shear flows over combined spatially and temporally structured walls	June 1998
882	Short, M., and D. S. Stewart	The multi-dimensional stability of weak heat release detonations	June 1998
883	Fried, E., and M. E. Gurtin	Coherent solid-state phase transitions with atomic diffusion: A thermomechanical treatment—*Journal of Statistical Physics* (1998)	June 1998
884	Langford, J. A., and R. D. Moser	Optimal large-eddy simulation formulations for isotropic turbulence	July 1998
885	Riahi, D. N.	Boundary-layer theory of magnetohydrodynamic turbulent convection—*Proceedings of the Indian National Academy (Physical Science)*, in press (1998)	Aug. 1998
886	Riahi, D. N.	Nonlinear thermal instability in spherical shells—in *Nonlinear Instability, Chaos and Turbulence* **2**, in press (1998)	Aug. 1998
887	Riahi, D. N.	Effects of rotation on fully non-axisymmetric chimney convection during alloy solidification	Sept. 1998
888	Fried, E., and S. Sellers	The Debye theory of rotary diffusion	Sept. 1998
889	Short, M., A. K. Kapila, and J. J. Quirk	The hydrodynamic mechanisms of pulsating detonation wave instability	Sept. 1998
890	Stewart, D. S.	The shock dynamics of multidimensional condensed and gas phase detonations	Sept. 1998
891	Kim, K. C., and R. J. Adrian	Very large-scale motion in the outer layer	Oct. 1998
892	Fujisawa, N., and R. J. Adrian	Three-dimensional temperature measurement in turbulent thermal convection by extended range scanning liquid crystal thermometry	Oct. 1998
893	Shen, A. Q., E. Fried, and S. T. Thoroddsen	Is segregation-by-particle-type a generic mechanism underlying finger formation at fronts of flowing granular media?	Oct. 1998
894	Shen, A. Q.	Mathematical and analog modeling of lava dome growth	Oct. 1998
895	Buckmaster, J. D., and M. Short	Cellular instabilities, sub-limit structures, and edge-flames in premixed counterflows	Oct. 1998
896	Harris, J. G.	*Elastic waves*—Part of a book to be published by Cambridge University Press	Dec. 1998
897	Paris, A. J., and G. A. Costello	Cord composite cylindrical shells	Dec. 1998
898	Students in TAM 293–294	Thirty-fourth student symposium on engineering mechanics (May 1997), J. W. Phillips, coordinator: Selected senior projects by M. R. Bracki, A. K. Davis, J. A. (Myers) Hommema, and P. D. Pattillo	Dec. 1998
899	Taha, A., and P. Sofronis	A micromechanics approach to the study of hydrogen transport and embrittlement	Jan. 1999